AD-A095 354 PARKER (LEE W) INC CONCORD MASS F/G 1/2
AIRBORNE LIGHTNING WARNING SYSTEMS: A SURVEY.(U)
JUL 80 L W PARKER, H W KASEMIR F19628-79-C-0161
UNCLASSIFIED AFGL-TR-80-0226 NL

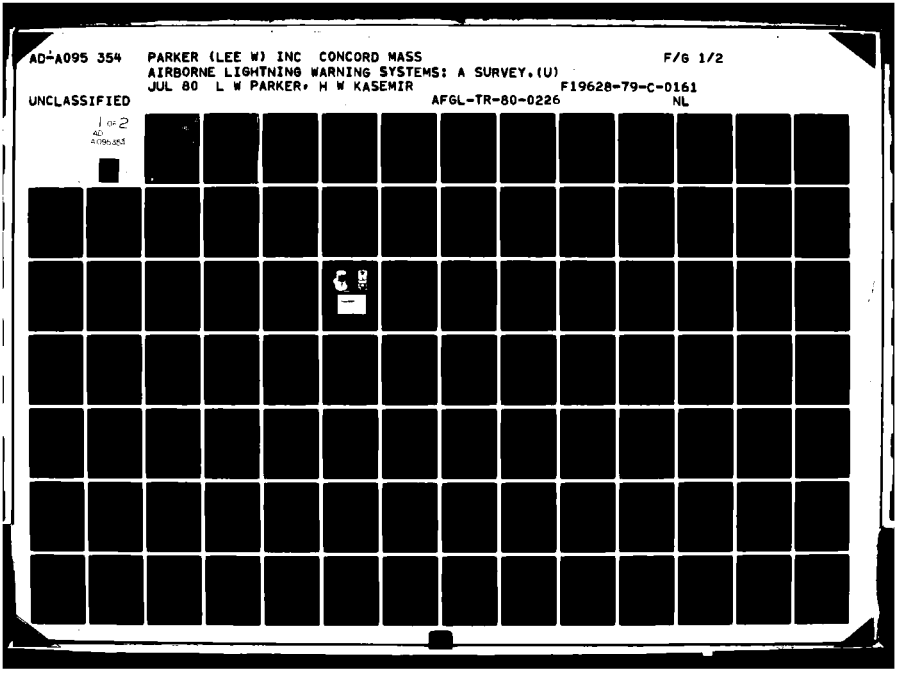

AFGL-TR-80-0226

AIRBORNE LIGHTNING WARNING SYSTEMS: A SURVEY

Lee W. Parker
Heinz W. Kasemir

Lee W. Parker, Inc.
252 Lexington Road
Concord, Massachusetts 01742

July 1980

Final Report
August 1979 to June 1980

This research was supported by the Air Force In-House Laboratory Independent Research Fund

AIR FORCE GEOPHYSICS LABORATORY
AIR FORCE SYSTEMS COMMAND
UNITED STATES AIR FORCE
HANSCOM AFB, MASSACHUSETTS 01731

Unclassified

SECURITY CLASSIFICATION OF THIS PAGE (When Data Entered)

19 REPORT DOCUMENTATION PAGE

READ INSTRUCTIONS BEFORE COMPLETING FORM

1. REPORT NUMBER (18) AFGL-TR-80-0226	2. GOVT ACCESSION NO. AD-A053354
3. RECIPIENT'S CATALOG NUMBER	
4. TITLE (and Subtitle) (4) AIRBORNE LIGHTNING WARNING SYSTEMS: A SURVEY	5. TYPE OF REPORT & PERIOD COVERED (9) Final Report. Aug 79 - Jun 80
	6. PERFORMING ORG. REPORT NUMBER
7. AUTHOR(s) (10) Lee W. Parker, Heinz W. Kasemir*	8. CONTRACT OR GRANT NUMBER(s) (15) F19628-79-C-0161
9. PERFORMING ORGANIZATION NAME AND ADDRESS Lee W. Parker, Inc. 252 Lexington Road Concord, Massachusetts 01742	10. PROGRAM ELEMENT, PROJECT, TASK AREA & WORK UNIT NUMBERS (16) 61101F ILIR9EAA (17) 9E
11. CONTROLLING OFFICE NAME AND ADDRESS Air Force Geophysics Laboratory Hanscom AFB, Massachusetts 01731 Monitor/Pio J. Petrocchi/LYW	12. REPORT DATE (11) Jul 80
	13. NUMBER OF PAGES 106
14. MONITORING AGENCY NAME & ADDRESS (if different from Controlling Office) (12) 108	15. SECURITY CLASS. (of this report) Unclassified
	15a. DECLASSIFICATION DOWNGRADING SCHEDULE

16. DISTRIBUTION STATEMENT (of this Report)

Approved for public release; distribution unlimited

17. DISTRIBUTION STATEMENT (of the abstract entered in Block 20, if different from Report)

18. SUPPLEMENTARY NOTES

*Colutron Research Corporation, 5420 Arapahoe Ave., Boulder, CO 80303

This research was supported by the Air Force In-House Laboratory Independent Research Fund

19. KEY WORDS (Continue on reverse side if necessary and identify by block number)

Aircraft instruments for lightning detection (accuracy)
Lightning detection errors
Instruments for lightning detection and warning
Sferics range and bearing detectors
Thunderstorm avoidance systems

20. ABSTRACT (Continue on reverse side if necessary and identify by block number)

Lightning warning systems for airborne use may be classified in accord with their application as ~~(a)~~ near-zone warning systems, and ~~(b)~~ distant warning systems. The near-zone systems considered here are essentially electrostatic field detectors (field mill, radioactive probe, and corona point) that can warn of the presence not only of thunderstorms but of high electric fields associated with nonthundery clouds that may nevertheless cause triggered strikes to aircraft (far outnumbering strikes due to natural lightning,

DD FORM 1 JAN 73 1473 EDITION OF 1 NOV 65 IS OBSOLETE

Unclassified 391800

SECURITY CLASSIFICATION OF THIS PAGE (When Data Entered)

according to pilot reports). Lightning-strike and high-field statistics, and associated corona effects, are discussed in connection with triggering of strikes. The distant warning systems considered, aside from airborne weather radar, include RF electric and magnetic sferics detectors, as well as optical systems and the above-mentioned near-zone detectors modified to also detect sferics. The sferics detectors sense electromagnetic fields radiated by lightning and by pre-lightning discharges, and may be classified according to their application as single-station bearing detectors (crossed loops-wideband or narrowband, multiple loops, time-of-arrival and interferometer systems), and as single-station range detectors (crossed loops, 500-kHz-pulse-height, spectral-amplitude-ratio/group-delay-difference, electric amplitude, e.g. $1/r^3$, and ratio-of-magnetic-to-electric-amplitude systems). Many of the systems surveyed have virtues warranting their consideration, as individuals or in combinations, for airborne warning and avoidance application. However, they all have advantages and disadvantages that require further investigation, careful testing and evaluation.

Serious errors in magnetic-crossed-loop bearing detection can be caused by (a) slant or inclination of the lightning channel, and by (b) secondary magnetic fields due to eddy currents induced by the incident magnetic field in the aircraft skin (site error). Both of these types of errors are treated analytically, leading to formulas and tables of site-error-correction factors for simplified aircraft models. Errors in single-station range detection can occur because of lightning source strength variability. The analyses of this report should be helpful in recognizing errors and suggesting improvements.

TABLE OF CONTENTS

TABLE OF FIGURES

TABLE OF TABLES

I. INTRODUCTION

The present survey was undertaken because a need exists for reliable and inexpensive (light-weight) airborne lightning warning and avoidance systems. Two applications of warning systems would be in (a) warnings of distant storms, enabling a pilot to avoid severe weather and possible encounters with hail, ice and dangerous air motions, and in (b) warnings of possible imminent lightning strikes to the aircraft in electrified clouds. Use of the familiar airborne weather radar is relatively straightforward with respect to (a), but not with respect to (b). One disadvantage of airborne weather radar is its relatively high cost. Another is the difficulty sometimes encountered, due to attenuation-masking effects, in identifying thunderstorms hidden behind heavy showers.

Potentially valuable adjuncts to, and possible inexpensive substitutes for, airborne weather radar are lightning detectors. These can be electrical or optical in nature. By detecting the electromagnetic radiation emitted by lightning and predischarges ("atmospherics" or more briefly "sferics"), RF detectors can warn of the existence of electrical activity at a distance. The electrical activity is usually associated with severe weather. Distant lightning warning can also be provided by optical detection of lightning flashes.

Another class of detector provides near-zone warnings. These are electrostatic field detectors that can be useful for warning and avoidance of lightning strikes to the aircraft. They warn of the presence of high electric fields. High electric fields exist, not only in thunderstorms that may already contain lightning, but also in non-thundery clouds where their presence may cause the aircraft to inadvertently trigger a strike. It may be inferred from pilot reports that these triggered lightning incidents outnumber by far the natural lightning strikes.

Lightning strike and electric field statistics, and some physical background on lightning triggering by aircraft, are considered in Sec. II. As candidates for electrostatic field detection instrumentation, we consider in Sec. III field mills, radioactive probes, and corona points. These have attractive characteristics, and all have been operated on aircraft.

Section IV deals with RF (sferics) instrumentation for detection of distant lightning. Among the sferics detectors considered as possible candidates for adaptation to airborne use as bearing detectors are crossed loops, multiple loops, a time-of-arrival (TOA) system and an interferometer system. The crossed and multiple loops have already been operated on aircraft, while the TOA and interferometer have only been operated at the ground. Nevertheless, the TOA and interferometer systems appear to have high potential accuracy and could be considered for adaptation to airborne use. They need further investigation, however. The multiple loops may also be considered, but they also need further investigation.

The crossed loop is a well-known direction finder. The commercially available narrowband version called Stormscope is apparently simple and low in cost. However, field tests (both airborne and ground-based) made to date raise questions regarding its accuracy and reliability. Moreover, details of the physical basis for its data-processing operations are not available. Therefore, more extensive tests should be carried out. In this connection the general analysis in the present report (Sec. IV and the Appendices) of crossed loops as bearing and range detectors should be helpful in recognizing errors and in suggesting improvements.

Another commercially available crossed loop system (Lightning Location and Protection) employs wide-band electronics and gates on the initial part of return-stroke signals. It is ground-based and is presently deployed for lightning-caused forest fire detection.

As a single-station range detector the crossed loop would be expected to be inaccurate in its present state of development which apparently assumes a $1/r$ dependence of the magnetic amplitude. Inaccuracies would be due in part to (a) lightning source variability, and in part to (b) site error (skin) currents.

Bearing errors analyzed in this report include the effect of slant or inclination in (non-vertical) lightning radiation channels, the effect of ground reflection (ionospheric reflection effects are considered negligible), and the effects of eddy currents induced in the aircraft skin that produce distortions in the local magnetic intensity vector. The channel slant and skin eddy currents both change the apparent source direction. Large errors can be introduced when the channel slant angle is large. (This type of error

can be minimized in the case of return strokes by employing gated wide-band (GWB) electronics.) In the case of the other type of error (site error) the skin currents can cause bearing errors (site errors) of about 20^{o} even if the loop is symmetrically located on the fuselage. The error can be larger if the instrument is mounted near the nose, a wing edge or a vertical fin edge. The distortion of magnetic field amplitude would cause errors in range detection by instruments relating magnetic amplitude to distance.

The narrowband crossed loop also has a 180^{o} ambiguity. This can be removed by using an electric field antenna in conjunction with the loop. However, electrical noise or uncontrolled phase shifts in the electronic circuits may make the system unreliable. A GWB return-stroke system may not have this need.

The multiple loops, TOA and interferometer may be less susceptible than the crossed loop to bearing errors due to lightning slant. However, they may be equally susceptible to site errors, and this should be investigated. If these instruments prove to have high accuracy and insusceptibility to errors with respect to bearing, multiple-station versions of these systems mounted on aircraft could be considered for lightning location by triangulation.

With respect to single-station range detection, 4 possible systems are considered besides the crossed loops, namely, an electric amplitude detector, an H/E amplitude ratio detector, a 500 kHz pulse-height-analysis detector, and a waveguide-propagation analyzer (low-frequency dispersion characteristics of the earth-ionosphere waveguide). All of these have attractive features and should be investigated.

Optical systems as bearing detectors are considered in Sec. V. Several possible constructions are suggested. In principle an optical detector would appear to have a minimal bearing error for a vertical lightning channel, but cloud illuminations by reflection/scattering of the light over extended regions (e.g. "heat" or "sheet" lightning) would spread the apparent source and make the direction correspondingly uncertain. An optical system is inexpensive and simple, however, and can be used for example in conjunction with one of the range detectors.

Section VI discusses airborne radar, the masking problem, and relations of precipitation echoes to lightning.

A summary of all systems considered for airborne use is given in Sec. VII, together with some tentative rankings. The systems are ranked according to availability, simplicity of construction, maintenance, calibration and interpretation of data, extent tested, potential accuracy, versatility, and insusceptibility to errors. The versatility category is of interest in

that some instruments can have more than one function, e.g., both range and bearing detection, or both near-range and far-range detection.

The appendices deal with "misdirection" analyses for crossed loops, i.e., the bearing errors due to slant lightning, and due to the distortion in the local magnetic field by induced skin currents (causing site errors). By a combination of theory and experiment one may determine correction factors for site errors affecting a crossed loop, for any given airplane geometry. The results of this determination would suggest optimum locations for the placement of the loop on the airplane. The correction factors need be determined only once. If this is done, the site errors can be completely eliminated by suitable adjustment of the electronic amplification. As an illustration, analytical correction formulas are given in Appendix B for various simple analytical aircraft models, including tabulations for a fuselage modeled by a prolate spheroid.

A better representation of the geometric form of an airplane can be obtained by computer modeling. An example of this is given at the end of Appendix B, where computed site errors for a T-39 airplane are discussed. General agreement is found between the results of the simple analytical model and those from the computer model. Nevertheless, more detailed information associated with the complex form of the airplane can be obtained from the computer model.

II. LIGHTNING STRIKE AND FIELD STATISTICS

A. Strike Statistics

In the last few years a large amount of information on lightning strikes to aircraft has been collected and reported in the literature (Corn, 1979; DuBro, 1980; Fisher and Plumer, 1977). Newman and Robb (1977) provide the following brief statement on airline pilot surveys: "Recently studies by Hourihan (1974) and Plumer and Perry (1975) have provided fairly extensive data on lightning strikes to modern jet airliners. According to Hourihan, over 80% of the strikes occurred within clouds, in precipitation and in turbulence. In over half of the strikes, St. Elmo's fire (corona) was observed before the strike. Most strikes occurred near the freezing level, from $-5^{o}C$ to $+5^{o}C$, and generally while descending or ascending through about 3 km altitude." This reflects the awareness of the fact that lightning definitely is a hazard to commercial as well as military aircraft. Ways and means have to be found to minimize the lightning danger to flight personnel and passengers, the lightning damage to airplanes and electronic equipment. For example, fly-by-wire and digitally-controlled aircraft may be extremely vulnerable. Prior to evaluating the advantages and limitations of the different warning systems to be discussed later, it will be worthwhile to assess certain aspects of the papers referenced above under the point of view of this report.

First we may resolve a certain controversy between pilots who report that lightning discharges are somehow caused by the aircraft and the scientists who discount these reports on the simplistic basis that sufficient charge cannot be stored on an aircraft to account for the energy required. The pilot observations may be found in a United Airlines report (Harrison, 1965). The situation is best described by Clifford (1980) as follows:

"The pilots almost unanimously agreed that there are two distinct classes of lightning observed in flight. The most common variety usually occurs while flying in precipitation at temperatures near freezing. This type is preceded by a buildup of static noise in the communication gear and the presence of corona (St. Elmo's fire) can be observed if the flight is at night. The buildup may continue for several seconds before the discharge (lightning strike?) occurs. The discharge terminates the static and corona.

The second variety occurs abruptly with no warning. It is most likely to be encountered in or near thunderstorms, in contrast to the former variety which is more likely to be experienced in precipitation that has no connection with thunderstorms. Pilots tend to believe that the slow buildup type of discharge is not a true lightning strike but rather a discharge of excess charge built up on the aircraft by flying through the precipitation. This non-thunderstorm type greatly outnumbers the other. Both kinds can create a brilliant flash and a boom which can be heard throughout the airplane.

The response of scientists to the pilot's static discharge theory has been universally negative. They insist that insufficient charge can be stored on an aircraft to produce a discharge which looks and sounds like lightning. Scientists are even more emphatic that insufficient energy could be contained in such a static charge buildup to produce any visible evidence such as burn marks, pitting or other damage on the aircraft. Yet, the pilots continue to insist that the aircraft is discharging and that the discharges do manifest themselves by bright noisy arcs and (not all pilots are sure about this) visible damage. The controversy has been characterized as a difference in view between scientists of long standing and pilots of long sitting."

We believe that the aircraft can trigger a lightning strike in an external field with no charge at all on the aircraft. In support of this assertion we propose the following hypothesis.

After the Apollo 12 incident, where the rocket was struck by lightning twice, it was pointed out by one of us (HWK) in a letter to Kennedy Space Center personnel that the Apollo spacecraft was not struck accidentally by two lightnings generated by a cloud that otherwise did not produce lightning discharges, but that the rocket triggered these lightnings by itself, upon penetrating high electric field regions in the cloud. This explanation was immediately accepted by Kennedy Space Center as well as the scientific community, because the alternative, namely that the cloud waited just to countdown zero and then fired two lightning bolts at the rocket while not being capable of producing other lightning discharges before or after launch, is too remote to be considered seriously.

Thus, what the pilots call the "common variety" of strikes to the aircraft, namely those that are preceded by corona discharge, are triggered lightning discharges caused by the airplane penetrating regions of high electric field. The rare variety, that occurs without warning, is an accidental hit of the airplane by a natural lightning that originates somewhere else in a thunderstorm.

Since such a distinction has far-reaching consequences in dealing with the aircraft lightning problem, we will discuss briefly some basic features of a lightning discharge that are relevant to the triggering problem (but that may not be widely accepted or even recognized). The electric field in a thunderstorm is usually not high enough to reach the breakdown value of 2000 to 3000 kV/m (the lower values occurring at higher altitudes). However, a raindrop, being electrostatically similar to a conductive sphere, has a field concentration factor of 3 at the upper and lower points (at its "poles") in the direction of the thunderstorm field. Therefore the external field necessary to cause breakdown there is reduced by a factor of 3. In addition to this the raindrop will deform into a spheroidal shape under the influence of the field, and the field concentration factors at the poles or tips will increase accordingly. Values of 5 to 10 may be reached by this deformation. This brings the thunderstorm

field required to produce breakdown at the tips down to values of 300 to 400 kV/m, e.g. values that have been measured in thunderstorms. If breakdown is reached at the tips of an elongated raindrop the raindrop will go into corona discharge. In this stage the raindrop is similar to an airplane in that corona discharge is observed by the pilots before a lightning is triggered. The corona discharge is a relatively stable discharge and without a further energy input the plane as well as the drop would remain in corona discharge until the external field drops below the breakdown value. The plane could obtain an additional energy input for instance by the impact of raindrops or ice crystals on the airplane skin or, in the absence of precipitation, by entering a higher field region.

With the additional energy input the stable corona discharge turns into an unstable spark discharge, e.g. a lightning discharge. Note that it is not necessary that the airplane be charged with an amount of charge usually associated with a lightning discharge. A minute fraction thereof is enough to turn corona discharge into a spark discharge. If this is achieved the energy required to let the spark grow into a lightning discharge is supplied by the thunderstorm field. This explanation should remove the objections of the scientific community, especially since the same principle works even for a raindrop. A raindrop already in corona discharge may acquire an additional energy input by a close approach to another raindrop, forming with it a conductive filament of doubled lengtn, or by being swept by turbulence, updrafts or downdrafts into regions of higher field strength. If the additional energy input is enough to turn corona discharge into a spark discharge -- or in lightning terminology into a streamer -- this streamer has a good chance to grow into a lightning discharge. The energy for this growth is again furnished by the thunderstorm field.

Needless to say, this picture of the sequence, corona discharge-streamer-lightning discharge, is an oversimplified sketch of a rather complex problem in plasma physics. It is sufficient for our purpose here to point out the similarity of a natural lightning triggered by precipitation particles and the lightning triggered by an airplane labeled as "common variety" by the pilots. The difference between these two events

is the greater capacity and field concentration factor of the plane. Consequently the airplane may trigger lightning discharges in electric fields that are much lower than those required to produce natural lightning discharges. This fits in with the pilots' observation that electric discharges triggered by airplanes in non-thundery clouds outnumber those occurring in thunderstorms. Probably hidden in this observation is the fact that thunderstorms can be recognized, and therefore avoided, by the presence of natural lightning discharges, whereas the presence of high electric fields cannot be detected by visual observation. If the airplane goes into corona discharge (visible only at night) it may already be too late for evasive action. In addition, there is no information to be gained from a single corona discharge on the fastest way to get out of the high field region. It has already been mentioned in an earlier report of this contract that all thunderstorm warning devices based on the electromagnetic waves emitted by lightning discharges are blind to the presence of electric fields too low to produce natural lightning but high enough to produce airplane-triggered lightning discharges. Instruments capable of detecting distant lightning as well as electric fields are the field mill, the radioactive probe and the corona point, which will be discussed in the next section.

The variety of lightning strike that occurs abruptly and without warning is rare according to the pilot reports. This is the case where the plane is accidentally in the path of a natural lightning. The lightning is extremely shortsighted. It would take no notice of the plane if its intended path passes the airplane at a distance greater than several lengths of the airplane body, say in rough figures greater than 100 m. If we define the target area as a circle with a radius of r=100 m = 0.1 km, the target area T is about $T=3\times10^{-2}km^2$. Let us assume that the cross section of a thunderstorm where natural lightnings occur is $S=6\times6\ km^2 = 36\ km^2$. Therefore, if we assume that lightning is approximately equally distributed over the thunderstorm cross-section, the probability P of a hit is given by the ratio of target area to thunderstorm cross-section, i.e., P=T/S=1/1200. This figure would be further reduced if we take into account that a lightning lasts only for about one second, i.e., to produce a hit the timing has to be exactly right. This may explain why a strike of an airplane by a natural lightning should be a rare event indeed.

The second observation of the pilots of the abruptness of the strike fits the data of the velocity of a leader strike. Even the "slow" step leader advances with a velocity of about 10^5 m/s. The reaction time of a pilot (plus the response time of the aircraft to changes in flight controls) would have to be under 1/100 second to recognize and avoid a leader one km away coming towards the airplane, assuming in addition that the pilot is looking in the right direction and can see so far into the cloud.

In conclusion we may summarize the discussion above as follows:

1. The pilot observations cannot only very easily be reconciled with the scientific requirements of the mechanism of a lightning discharge including the energy problem, but may be considered as an excellent confirmation of some hypothetical assumptions concerned with the initiation of a natural lightning.

2. The emphasis placed by the pilots on the distinction between a static discharge (triggered lightning) and the abrupt lightning strike (natural lightning) should be adopted in all statistical evaluations. There are vast differences between the two types of discharges: available power, resulting damage, number and place of occurrence, and very probably frequency spectrum. The latter parameter may play an important role in the assessment of vulnerability of electronic equipment.

3. The notion that the airplane charge produced by impact of precipitation has to furnish the charge for a lightning discharge should be abandoned. However, the energy furnished by this charging process may play an important role in the conversion of corona discharge into a streamer leading to a triggered lightning discharge.

4. In 1946, L. P. Harrison suggested that "the field distortion or augmentation created by the presence of the aircraft may raise an initially high but sub-critical

potential gradient to the level where breakdown occurs at or near the aircraft. If conditions are suitable the streamer could then continue to propagate between charge centers and a discharge would occur." (Fitzgerald, 1967).

B. Field Statistics

We now turn to a discussion of the field distribution in a thundercloud (Figures 1 and 2, unpublished). Figure 1 shows a graph of the vertical gradient in a particular storm versus altitude or temperature. The horizontal axis gives the gradient from -200 kV/m to +250 kV/m. The vertical axis gives the altitude from about 3.8 to 6 km and has a temperature scale from +3 to -12°C. The data were collected by two airplanes equipped with field mills making repeated (26) storm penetrations at different altitudes during the NOAA lightning suppression project (Holitza and Kasemir, 1974; Kasemir et al, 1976). The base of the cloud was a 4 km altitude. The peak of the negative gradient of -150 kV/m occurred at about 4.9 km altitude at a temperature of -2°C; the maximum positive gradient of 200 kV/m occurred at 5.5 km altitude or the -10°C temperature level. The lower negative peak gradient indicates the altitude level where ground discharges would originate and the upper positive gradient where intra-cloud discharges would originate. However, both gradient values were in this case too low to initiate lightning discharges. It is remarkable that during the 26 storm penetrations neither the low altitude airplane, a T29, nor the high altitude B26 triggered a lightning discharge. It is of interest to note here that the thicknesses of the high-gradient layers are rather small, of the order of only 200 to 300 meters. This narrowness is even more apparent in Fig. 2. The vertical axis again gives the altitude; the horizontal axis represents time and is marked with the days from July 27 to August 21, 1974. On thunderstorm days measurements

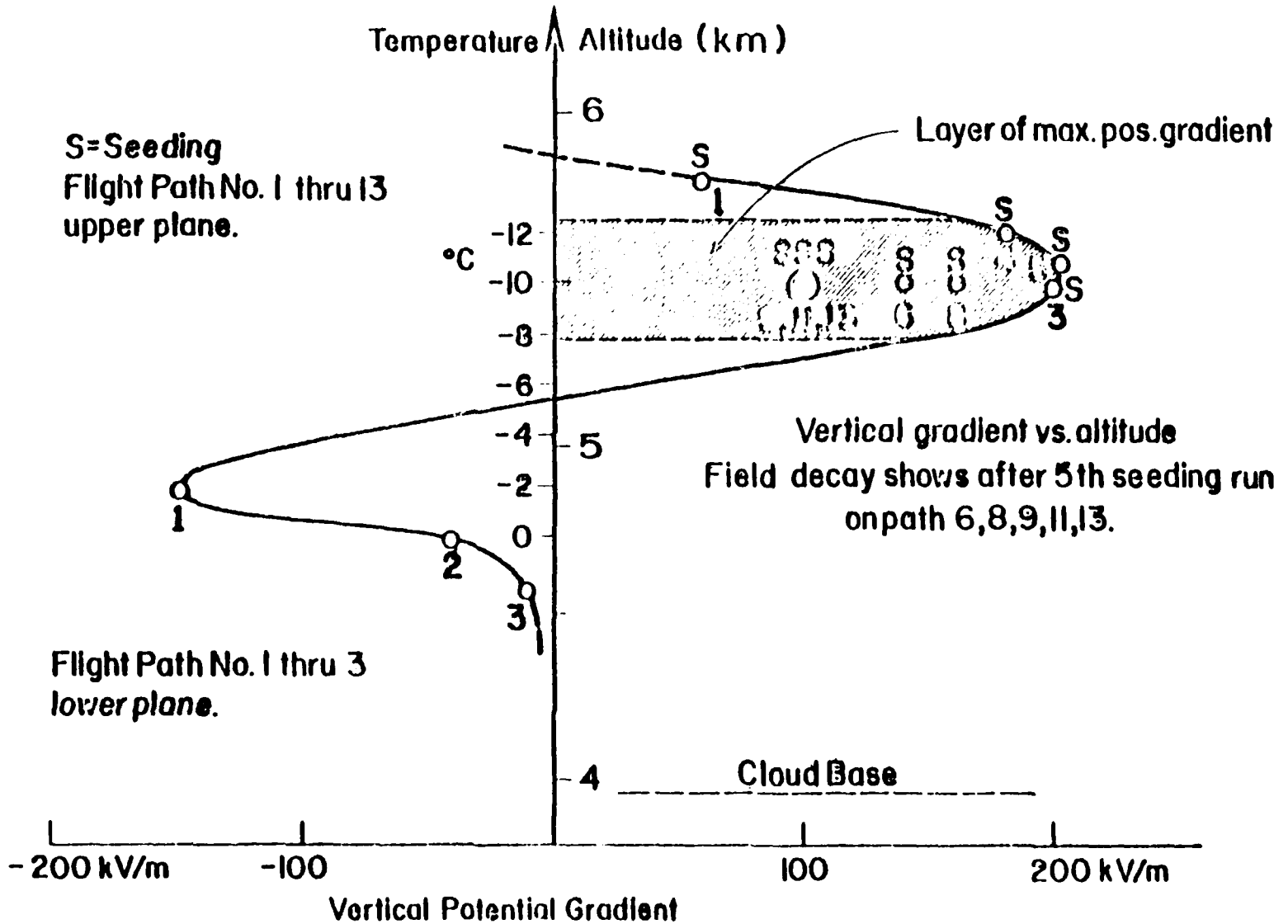

FIG. 1. Potential Gradient vs. Altitude in Thunderstorm

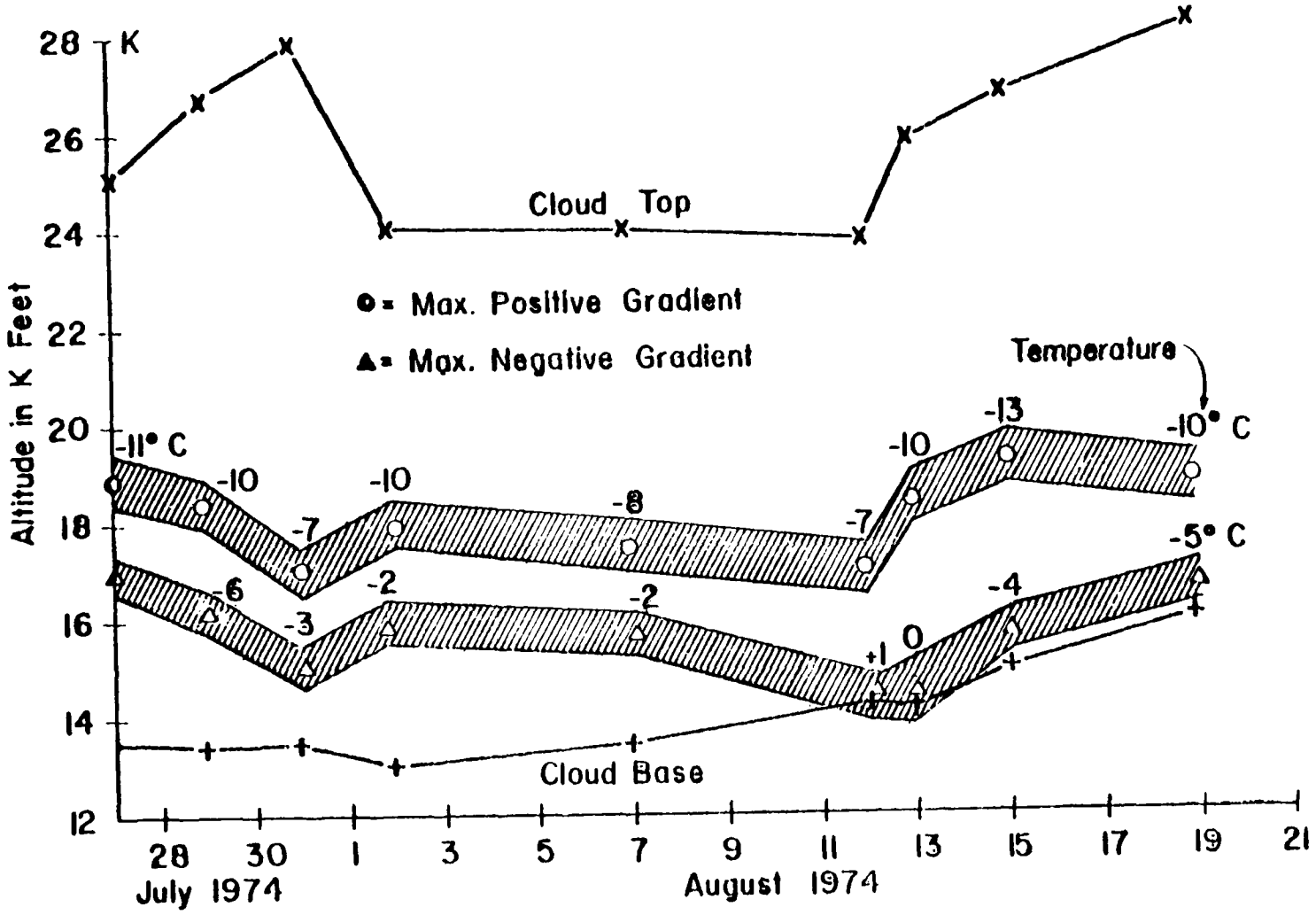

FIG. 2. High-Gradient Layers and Associated Temperatures in Thunderstorms

were carried out of the type discussed in connection with Fig. 1. In Fig. 2, however, only altitudes of cloud top and base (marked by crosses), of maximum positive gradient (marked by circles), and maximum negative gradient (marked by triangles) are given. The numbers above the gradient symbols indicate the temperature. The boundary lines of the shaded bands mark the 60 kV/m values enclosing the maximum positive gradient in the upper band, and the -60 kV/m gradient values enclosing the maximum negative gradient in the lower band. We see that maximum positive gradients have been located between the -7 to -13°C temperature levels, and maximum negative gradients between the +1 and -6°C levels. The thickness of the bands is about 1000 feet = 300 m. It is important to note that the temperatures as well as altitude levels of the maximum gradients are not fixed to an exact temperature or altitude but may change from day to day. The thunderstorms were small to moderate heat storms occurring in Colorado and Wyoming, with ground level about 5 kilofeet above sea level. A word of caution should be added regarding Figs. 1 and 2. The blank area in Fig. 2 between 20 and 28 kilofeet altitude does not mean that this layer doesn't contain high gradients. It simply means that this area could not be investigated because it was above the ceiling of the aircraft. (For gradient data at higher altitudes, see Fitzgerald, 1968.) It should also be mentioned that it is not easy to locate the high gradient areas. Without the records of all three components of the gradient provided by the field mills and by on-the-spot evaluation it could not have been done at all. Even so it is easily possible that some high gradient areas could have been missed, since they seem to occur in narrowly restricted regions. The importance of such data to avionics doesn't have to be stressed. The pursuit of this type of research to include different storms (frontal storms, severe storms, storms over land with lower elevation, storms over sea, storms in different seasons, nonthundery clouds, etc.) is highly recommended.

A tentative conclusion can be drawn from these figures (1 and 2). The thinness of the high gradient areas suggests that a quick change in altitude should be made if an airplane finds itself in the state of corona discharge. The change should always be to <u>higher</u> altitudes even though there is a chance of penetrating the higher positive-gradient layer. A

triggered lightning in the lower negative-gradient region may penetrate to the ground and involve the plane in a ground discharge. The lightning triggered in the upper high-gradient area will most likely be an intra-cloud discharge that doesn't have the destructive power of a ground discharge.

It is interesting to compare these figures (1 and 2) with the figures "Aircraft Lightning-Strike Incidence vs. Altitude," and "Lightning Strikes to Aircraft as a Function of Temperature," presented by Fisher and Plumer (1977) and reproduced here as Figs. 3 and 4. Most of the lightning strikes in Fig. 3 occur in an altitude range of 5 to 18 kilofeet and in Fig. 4 in a temperature range of -10 to $+6^{o}C$. The higher altitude and lower temperature boundary in Figs. 3 and 4 are in excellent agreement with the boundaries given in Figs. 1 and 2. However, the lower altitude (5 kilofeet) and higher temperature ($+6^{o}C$) boundary in Figs. 3 and 4 show a much lower altitude than the boundary (14 kilofeet, $+1^{o}C$) given in Fig. 2. This difference can be easily explained by the high ground level of 5600 feet above sea level in Colorado and Wyoming. Therefore within reason the agreement between the two sets of data has to be classified as good.

The significance of the agreement between the two sets of data is in the fact that the occurrence of two physically different events -- lightning strikes to aircraft and high gradients within clouds -- are correlated. They are linked together by the reasonable assumption that lightning discharges are initiated or triggered in the high-gradient areas. This result suggests the possibility of conducting detailed research on the probability of lightning strikes by using the safer and more effective method of locating the high-gradient areas in clouds rather than by provoking aircraft lightning incidents (although the latter is certainly a direct approach - see Pitts et al (1979) and Maxwell et al (1979)).

Another remark may be made in this connection. Lightning research, testing of instruments, etc., are often done in the laboratory with high-voltage sparks. This too is a safe and effective method. There is, however, a marked difference between a lightning discharge and a spark. The lightning is an electrodeless discharge that draws its power from the

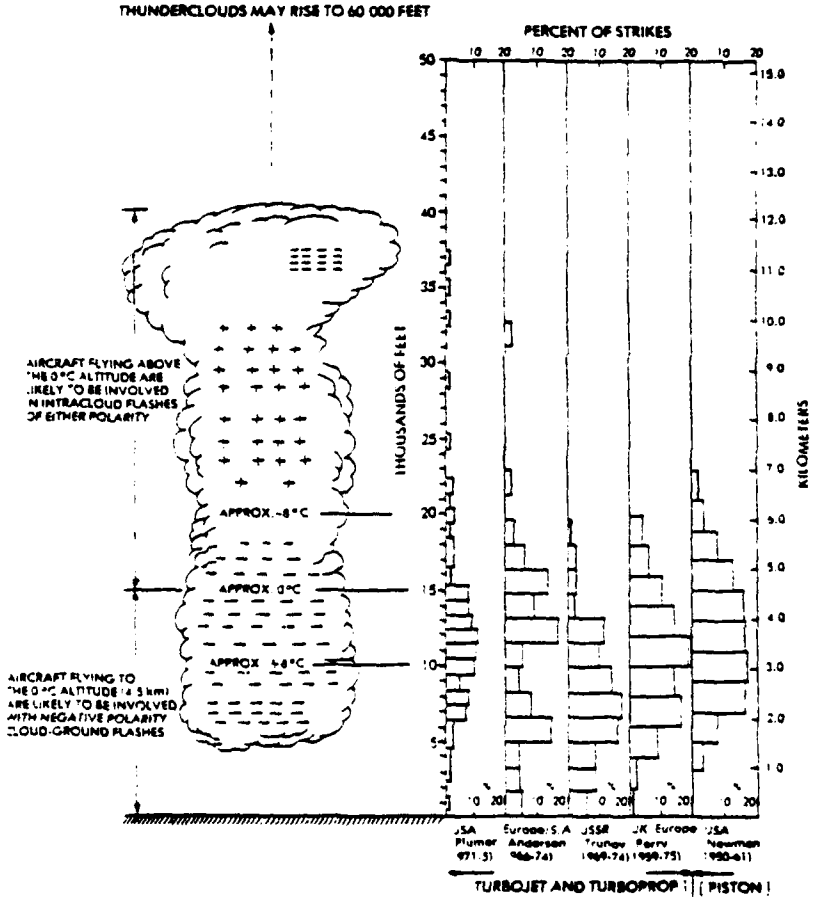

FIG. 3. Aircraft lightning-strike incidents vs altitude.

(Fisher and Plumer, 1977)

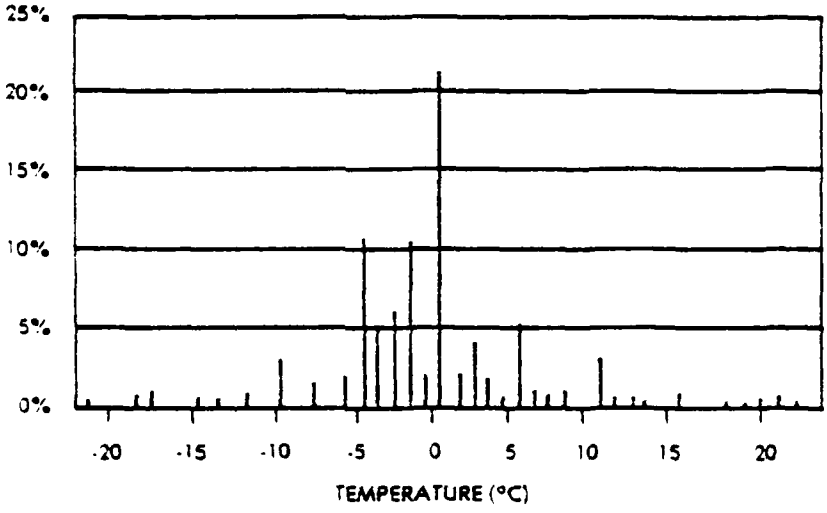

FIG. 4. Lightning strikes to aircraft as a function of temperature.

(Fisher and Plumer, 1977)

electric field of a space charge distribution in the cloud. Electrotechnically speaking, the power supply represented by an electrified cloud has a very different internal impedance than a high voltage generator. This internal impedance may exert a significant influence on the electrical characteristics of the lightning on the one hand or on the spark on the other hand. A similar difference exists in the theoretical modeling of a lightning discharge by a transmission line. The transmission line exists already before the current pulse is injected, and resistance, capacitance and inductance are constants that can easily be calculated. The lightning discharge has to build its channel by itself. Resistance varies strongly in space and time and is current-dependent. Therefore, Ohm's law (constant resistance) doesn't hold. In case of the capacitance and inductance, even a definition is difficult. (Therefore, use of the telegraph equation in theoretical approximations is not sufficient.) In the theoretical as well as laboratory modeling of a lightning discharge it would be highly desirable that some assurance be gained regarding how far results and conclusions can be applied to lightning problems. Theory would have to be extended to include plasma physics, and a check of laboratory tests should be made with real lightning discharges. This can be done by the use of a lightning tower or in our case by the more direct approach of provoking lightning strikes to test airplanes (Pitts et al, 1979; Maxwell et al, 1979).

Some relationships of lightning activity (and strikes to aircraft) to radar echoes have also been considered by Fitzgerald (1978). (See Sec. VI on meteorological measurements.)

C. Strike Statistics in Thunderclouds

Fitzgerald (1967, 1968, 1970) has analyzed data from instrumented aircraft penetrating thunderstorms during the 1965 Rough Rider program. Among his findings relevant to this section are the following:

1. Very high fields are not required for strikes to aircraft (390 kV/m was the maximum measured).

2. The currents of lightning strikes to planes were compared with those to power lines:

   Power lines: 50% above 15 kA, 10% above 40 kA
   Planes: 50% above 2 kA, 10% above 7 kA
   (largest current 22 kA, limited data)

3. In strikes to a F-100F aircraft, in normal behavior, sensors indicated electron current moving upward from the aircraft toward a positive charge region overhead, and electron currents upward toward the aircraft from a negative charge area below the aircraft.

4. Most strikes occurred while the aircraft was in transition from a region with positive charge above and negative charge below into a region with reversed polarity (negative charge above and positive charge below).

5. Strong fields (tens of kV/m) are encountered at high altitudes (-68^{o}C and 50 kilofeet).

6. Intense strikes were frequently associated with dissipating storms. Here we quote Fitzgerald (1967):

   "The data presented suggest that thunderstorms in their early stages of dissipation retain sufficiently large charge centers to account for one or more lightning discharges if a suitable means of initiating a streamer becomes available. It is likely that an aircraft entering a storm in this condition will act to 'trigger' a lightning discharge. These clouds may have little turbulence and no distinctive echo pattern on a typical Air Traffic Control radar. In normal IFR flight operations in regions with thunderstorms merged with showers and cloud decks, the routine radar avoidance of the presently most active storm portions may readily lead to flight through a decaying storm and the possibility of an isolated lightning incident to the aircraft."

D. Other Investigations

Thunderstorm penetrations with instrumented aircraft that were struck include those made by Cobb and Holitza (1968), Nanevicz et al (1977), and Musil and Prodan (1980). Their observations further corroborate those considered in this section.

E. Corona and Triggering

In an interesting set of relevant experiments, the effects of corona-producing points on the trigger-breakdown field of the shuttle-orbiter were investigated by Kasemir and Perkins (1978). They used a scale model of the spacecraft placed between the plates of a large plate condenser. As part of the investigation they also used a highly-polished spheroid to determine the trigger-breakdown field in the absence of, and in the presence of, corona-producing points on the spheroid. Two principal results are the following:

(a) the trigger-breakdown field is about 33% less with corona points than without, and

(b) the percent reduction of the trigger-breakdown field (33%) due to the presence of corona points is only weakly dependent on the nature of the points (form, length, sharpness, etc.).

An important ramification of these results regarding triggered lightning strikes to aircraft is that

(a) not only is the likelihood of a triggered strike enhanced (33% lower trigger fields) by the presence of corona (in addition to altitude-dependent reduction of the trigger field), but that

(b) all aircraft have so many sharp metallic protrusions acting as possible corona points (antennas, pitot tubes, landing gear, nuts, lightning arresters, exhaust nozzle rims, edges, corners, etc.) that they are essentially always in corona in strong fields.

III. FIELD MEASUREMENTS

We consider in this section 3 types of instruments for measuring electrostatic fields, all suitable for airborne use. We discuss first the field mill, then the radioactive probe, and finally the corona-point detector, all well-known instruments that have been used extensively for many years. A considerable amount of historical and technical data on these and many other instruments may be found in the comprehensive texts by Israël (1971, 1973) and Chalmers (1967).

A. Field Mills

The field mill is an electrostatic voltmeter, of rugged design but high sensitivity. This is an electrostatic induction type of instrument. A forerunner of the modern version was designed by C.T.R. Wilson (1920). There are many possible designs for such an instrument, e.g. planar-snutter field mill, cylindrical field mill, rotating wire, etc. In the same family of instruments as the field mill are the electrostatic fluxmeter (test plate moving, not fixed), induction voltmeter and agrimeter (test plate grounded when exposed, connected to measuring instrument when shielded - Chalmers (1967)). We will discuss two types, the planar-shutter field mill and the cylindrical field mill. The instrument is capable of measuring atmospheric electric fields over a wide range, from one V/m to 500,000 V/m. Since high electric fields are a characteristic feature of thunderstorms, the field mill is an ideal tool for thunderstorm research and is widely used for that purpose. Its capability of small and compact design makes it suitable for airborne application.

Briefly, in a planar-shutter type of field mill, a rotating grounded electrode alternately shields a fixed insulated electrode from, and exposes it to, the electric field external to the instrument. A diagram of this type of field mill is shown in Fig. 5a (from Chalmers, 1967). The a.c.

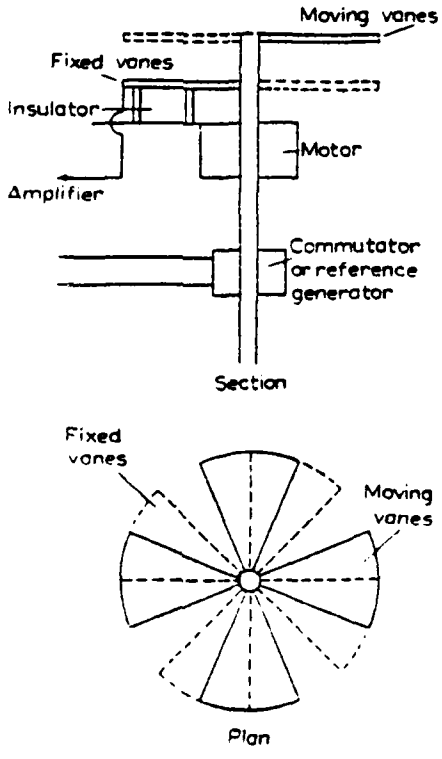

FIG. 5a. Field Mill Schematic (Planar-Shutter Type)

(Chalmers, 1967)

voltage output of the fixed electrode is proportional to the strength of the field. The planar-shutter type field mill was designed to measure the atmospheric electric field at the ground (see Israel, 1973). In this case the field has only a vertical component. The sensitivity is about 5 V/m. The instrument has a frequency range, the upper limit of which is determined by the rotation rate of the shutter and the number of vane sectors, that is, the frequency with which the openings are covered and uncovered. Typically, for example, the upper frequency may be 10 Hz for a 30-Hz rotation frequency. With a capacitive by-pass, however, the frequency range can be extended into the RF region and above (Smith, 1954). This means that short pulses "field changes" radiated by lightning discharges can be detected. The limitation here is given by the design of the electronic amplifiers, and not by the sensor head (i.e., the field mill proper).

In general, the electric field vector may be measured by using multiple field mills with different orientations to infer the three components of the field. At the ground, however, the electric field vector is normal to the earth's surface. Therefore, one field mill suffices to obtain the vector.

The extension of the ground field mill instrument to airborne operation involves a system of at least 4 field mills, mounted, if possible, at symmetric locations on the airplane surface, e.g., the two wing-tips, or the top and bottom of the fuselage, or similar positions. With an analog or digital computer circuit the four inputs can be analyzed, yielding the three components of the external field vector, separated from the field generated by the electrostatic charge on the airplane.

Airborne versions of the planar-shutter field mill have been designed and flown by Gunn (1933), Kasemir (1943), Clark (1957), and Fitzgerald (1965), and more recently by C. R. Holmes at New Mexico Tech and by D. Olson at the University of Minnesota.

The cylindrical field mill (Fig. 5b) was specifically designed for airborne use (Kasemir, 1972, 1978). Its rotating electrodes alternately shield and expose one another, but neither is grounded. Its sensitivity is one V/m, which gives it a larger range of detection of thunderstorms than the

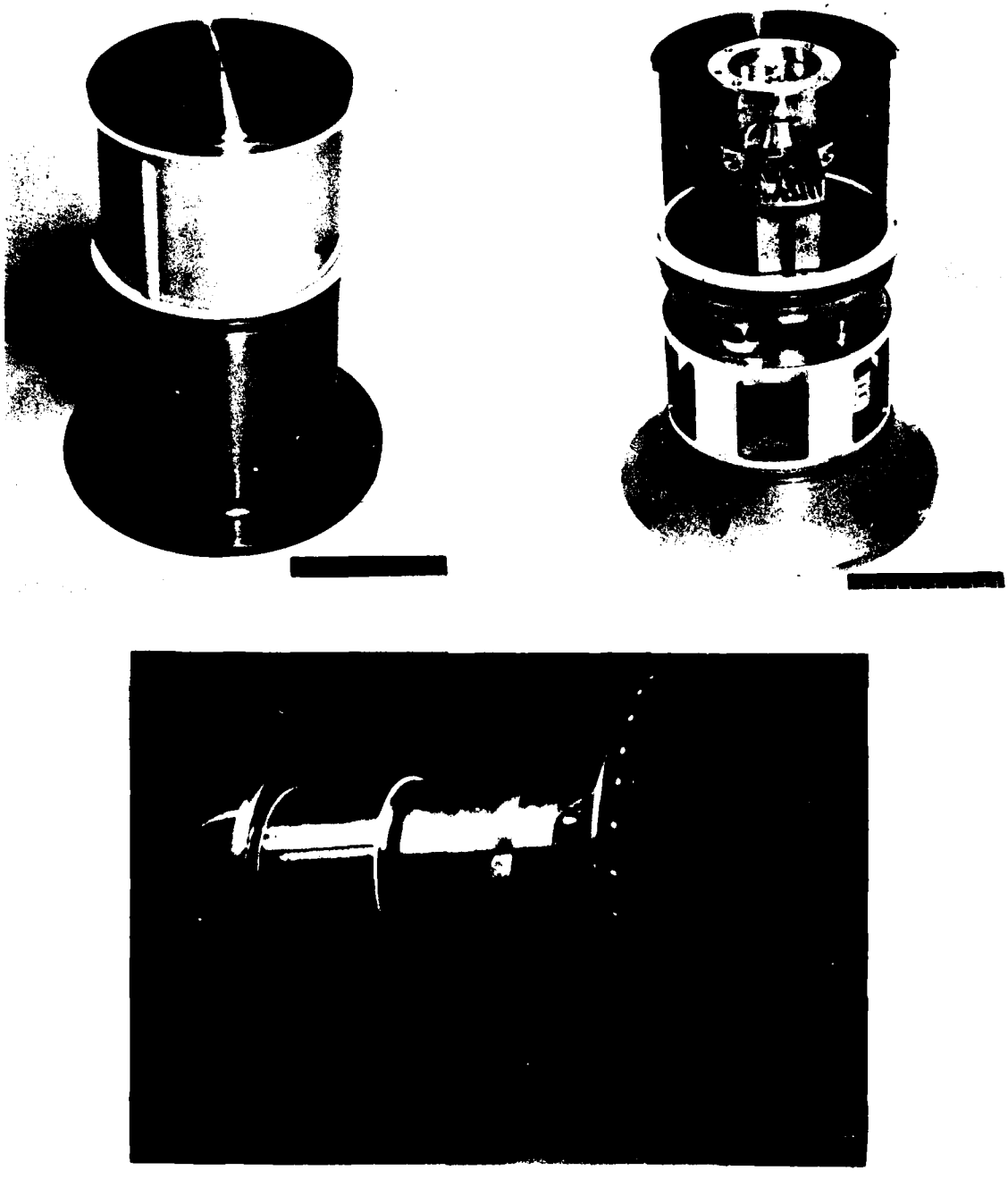

FIG. 5b. Cylindrical Field Mill

Upper left: Rotating split-cylinder sensor head (upper section), on stationary base (lower section). White strips are Teflon insulators.

Upper right: Opened sensor head, one cylinder segment removed.

Bottom: Mounted on airplane nose, with eccentric "humpring" charge compensator added. (Dark line along centerline is a reflection of unknown origin.)

planar-shutter type. The basic frequency range is also 0 to 10 Hz, with the above-mentioned extendability to RF frequencies via a capacitive by-pass. The cylindrical field mill has an important advantage in being much less influenced by the airplane charge. This influence can be reduced significantly by use of a charge compensator or "hump ring" (Kasemir, 1978).

On an aircraft, two cylindrical field mills are sufficient, one measuring two of the three components of the field vector, the other measuring the third component, plus one component already obtained by the first mill. This redundant measurement of one of the field components by both field mills has proven to be valuable and provides a continuous check on the proper operation of the field mills. Thus, two cylindrical field mills are equivalent to five shutter-type mills.

The vertical cylindrical field mill is sensitive to noise produced by rain because one of the sensitive cylinders is exposed to impact by rain. If the shutter-type field mills are mounted in such a way that none of them is facing the flight direction they are protected from direct impact of rain, and they are comparatively noise free.

An extensive planar-shutter type field mill network at the ground has been in operation at Kennedy Space Center for thunderstorm warnings during the launch of important rockets, for instance the Apollo series, the Mariner program, and so on. Many airplanes have been equipped with field mills for thunderstorm warning, and for thunderstorm and lightning research projects sponsored by federal agencies. For instance, 8 airplanes equipped with field mills participated at the Apollo-Soyuz launch at Kennedy Space Center. Other examples include projects conducted by the U.S. Army in 1956-1958, the U.S. Air Force Rough Rider lightning research project, the U.S. Navy fog research project, the NASA lightning triggering project, the NOAA lightning suppression project, and the TRIP projects 1976-1979. It should be mentioned that in the NASA lightning triggering project (rockets fired to trigger lightning), in the NOAA lightning suppression project (chaff seeding to dissipate the charge concentrations), and in the Air Force Rough Rider project (see Fitzgerald (1970), investigating probabilities of lightning strikes), the field-mill-equipped aircraft were used to locate the high-electric-field areas in the storm with the intention of penetrating and not avoiding these areas of maximum lightning probability.

If an airplane approaches a thunderstorm from a sufficient distance, the field is essentially that of the net charge of the storm. In this case it is not difficult to display on a cockpit meter the direction of the storm using the field vector. However, if the plane is inside or close to the storm the field pattern becomes more complex and a computer would be required to display the storm direction.

Compared with RF sferics sensors (discussed later, Sec. IV), the field mill is, in its static form, a short-range warning device capable of sensing fields and thunderstorms at distances up to about 10 miles. At this distance lightning discharge pulses are also clearly visible on the record. However, using the capacitive bypass or RF mode, the d.c. and ELF part of the signal is filtered out. This eliminates the capability of recording thunderstorm fields but increases the signal-to-noise ratio of the lightning field. Therefore, lightning discharges can be detected at distances up to 100 miles. It should be mentioned that the use of the d.c. and RF modes of operation are not mutually exclusive but can be used simultaneously in separate channels.

Besides providing lightning information, the field-measuring capability of a field mill has two distinct advantages. First, it warns of the possibility of triggered lightning in highly-electrified clouds that contain no natural lightning (see discussion in Sec. II). Such a situation occurred in the Apollo 12 incident, during which 2 lightning discharges were triggered by the rocket. Second, it warns of the production of corona discharge on the airplane that may interfere severely with communication. The field-vector display in the cockpit would in both cases indicate the direction away from the high-field area.

An absolute calibration of an airplane field mill system requires time and effort at installation. Since the field mill is used mostly as a scientific instrument, its calibration, accuracy, response, etc. problems are fully recognized and dealt with. The same problems exist also for the calibration of RF sensors. However, in this case the necessity of calibration is often disregarded as being of minor importance, or sometimes not even recognized as existing. This results in bearing and range errors discussed later. Because of the similarity of the problem much can be learned regarding RF sensor calibration from field mill calibrations. However, to date one has been content here with a coarse empirical calibration, and errors, for instance site errors discussed later, remain usually unrecognized.

B. Radioactive Probes

Radioactive probes (collectors) have long been used to measure the potential of a point in space with respect to the ground potential, even before the electron tube was invented (see Israel, 1973). The potential difference divided by the height above ground gives the potential gradient, provided the gradient is constant. The probe operates by ionizing the surrounding air within a roughly spherical region, of radius about 5 cm at sea level and 10 cm at 10 km altitude. The ionized and slightly conductive air discharges or charges the probe until its potential is essentially equal to that of its near environment. Parachute dropsonde versions were used in 1928 and 1940, and a radiosonde in 1942 (Israel, 1973).

The amount of radioactive material involved depends on the material used. Typically, 10 microcuries of radium or 100-500 microcuries of polonium may be used. Polonium is a pure alpha-emitter and is considered safe (used commercially to prevent static charging on phonograph records).

In principle this is an extremely simple device. However, there are a number of problems that have to be considered in the construction of a field measuring device using radioactive probes. Some of these are the following.

The probe must be well insulated from the ground (or airplane surface). The insulation requirement is severe: insulation resistance should not be less than 10^{13} to 10^{14} ohm. The slightest film of moisture due to humid air, condensation, etc., would short-circuit the probe to ground. (However, Teflon is a hydrophobic insulator, and with it the problem may not be too severe (R. Markson, personal communication).)

The load placed on the radioactive probe must have impedance of the order of at least 10^{12} ohm so that the probe can maintain its open-circuit voltage. In presently-available technology this dictates the use of field-effect transistors (FET's) as first-stage amplifiers. These amplifiers can handle comfortably input voltages in the range from millivolts to several tens of volts. However, they would be damaged by 50 V or 100 V at their input terminals. On the other hand, a radioactive probe located at 50 cm

above ground would supply in normal fair weather of 100 V/m an input voltage of 50 V. In a moderate thunderstorm field of 10 kV/m, it would supply an input voltage of 5 kV.

Hence the FET amplifier requires a high-ohmic voltage divider to reduce the input voltage. However, high-ohmic resistors have not only a temperature coefficient but also a voltage coefficient. That is, their resistance value drops significantly for voltages higher than about 1000 V.

In addition, the radioactive probe itself saturates at fields on the order of 5 kV/m.

In spite of all these problems the radioactive probe is used as a field meter since it also has some unique advantages. It and the corona detector (below) are to our knowledge the only field-measuring devices that have no moving parts. It is of light weight, and has negligible power requirements including the electronics. Its construction costs are very moderate. It is essentially a fair-weather instrument, but its capability for measuring small fields down to one V/m or less would make it useful for detection of thunderstorm fields at a large distance.

Radioactive probes have been operated successfully on aircraft outside clouds by Vonnegut et al (1961) and Markson (1976). In the only airborne comparison test known to us in which a radioactive probe system and a field mill system were flown simultaneously on two separate airplanes flying side by side, the radioactive probe data and field mill data tracked each other extremely well (Kasemir, 1978).

C. Corona Detector

The relation between the current I flowing from a corona point and the electric field E producing the corona discharge is given, according to Whipple and Scrase (1936), by

$$I = a\,(E^2 - E_0^2); \quad E \geq E_0 \qquad (1)$$

where a is called the "corona constant" and has an empirical value in the range 10^{-13} to 10^{-16} A-m^2/V^2. Corona discharge does not start until the field at the corona point exceeds the breakdown value in air. The ratio of the field at the point to the corona-producing field E is the field concentration factor. This factor is fairly constant for the individual point but it depends on the height of the point above ground, usually given by the length of the rod carrying the point, and on the radius of curvature at the point. Therefore, large differences in the field concentration factor exist from point to point.

The field concentration factor determines the onset field E_o, which has a value of about one kV/m for a field concentration factor of 3000. If the external field E is smaller than the onset field the corona current is zero (not negative). The onset field and corona constant for positive fields differ by about 10 percent from those for negative fields. Moreover, these parameters depend on the wind. This wind dependence in airborne applications has been thoroughly investigated by Chapman (1958).

An intensive study of corona discharges has been made by Loeb and his co-workers (Loeb, 1965).

Balloon-borne corona points were used as early as 1937 and 1941 by Simpson and Scrase (1937) and Simpson and Robinson (1941) to determine the polarity of electric fields in thunderclouds. More recently measurements of thunderstorm fields using corona points were made by Weber and Few (1978) using balloon-borne ("coronasonde") payloads, and by L. Ruhnke (1971b) using Mighty Mouse rocket-borne payloads. At Ruhnke's suggestion, R. Markson (personal communication) complemented his airborne radioactive probe system by an equivalent corona-point system, in order to extend the field-measuring range of the radioactive probes to higher field values. Markson's results showed that the two systems tracked one another well in their overlap range (R. Markson, personal communication).

The combination of these two devices (radioactive probes and corona points) deserves further investigation. Both systems are simple and light-weight. The corona points have the advantage of being operated in the short-circuit mode and therefore do not need high-ohmic insulation.

They have the additional advantage of being rugged and fairly immune to rain or humidity. Furthermore they would be more sensitive to corona discharge than the communication equipment of the airplane, and can be designed as a system to measure all three components of the electric field vector.

D. Extension to Long-Distance (Sferics) Detection

As with field mills, radioactive probes and corona detectors are primarily short-range warning devices, but can be extended to also detect RF pulses from distant lightning. The extension again consists of using capacitive by-passes. The rod used to mount the radioactive probe or the corona point would serve as an antenna for lightning RF signals.

IV. SFERICS DETECTORS

The electromagnetic radiation emitted by a lightning discharge is usually known to radio or TV users as "atmospherics" or "sferics". It can be used in different ways to determine the direction of the source of the emission, i.e., the lightning discharge. We will consider here crossed loops. TOA systems and interferometer systems will be discussed in a later section ("Special Systems").

A. Crossed Loops as Direction Finders

Low-frequency direction-finding by narrowband magnetic loops is a rather old and well-known technique (e.g. Watson Watt and Herd, 1926). The theory of the magnetic crossed loop is as follows.

A time-varying magnetic field penetrating the area enclosed by a wire loop will induce in the wire a voltage and current proportional to the time variation and strength of the magnetic field and to the area of the loop. If the normal vector of the loop surface and the magnetic field vector are parallel the induced voltage is a maximum. If the two vectors are orthogonal the induced voltage is zero. At an arbitrary angle of incidence α the induced voltage depends on the cosine of the angle α. If there are two loops whose planes are at right angles to one another (crossed loops) the induced voltages in the two loops are proportional to $\cos\alpha$ for one loop and to $\sin\alpha$ for the other loop. The ratio of the two loop voltages is a function of the incidence angle α, but not of the magnetic field strength since this cancels out. From this ratio, therefore, the azimuthal direction of the lightning discharge is easily determined. Note that only two components of the magnetic vector can be detected with a crossed-loop antenna. Since the antenna is usually mounted on top of the fuselage the visibility of the crossed loop is limited to the horizontal plane. Only D. Kohl (1966) has attempted to obtain all 3 components of the magnetic vector with his multi-loop antenna. (See discussion on p. 41.) There remains, however, a 180-degree ambiguity in the two-loop system. This can be resolved by using an omnidirectional electric field antenna in conjunction with the crossed loops. However, electrical noise or uncontrolled phase shifts in the electronic circuits may make the system unreliable.

1. Use of Electric Antenna to Resolve 180-degree Ambiguity

A simple way of seeing how correlation of the phases of the electric and magnetic vectors can be used to resolve the ambiguity is the following.

Consider one loop of a narrowband crossed-loop system aligned with two sources, one in "front" and one in "back". In Fig. 6, the plane of the loop is perpendicular to the plane of the paper and is aligned with the sources (upper dot = front, lower dot = back). The sources are assumed to be electric dipoles in the same plane as the detector, but oriented perpendicular to the plane of the paper. Four sets of vectors are shown, at (a), (b), (c) and (d), with E, H, and P in each set denoting, respectively, the electric vector, magnetic vector, and direction-of-propagation vector, respectively. Sets (a) and (b) correspond to radiation from the front, while sets (c) and (d) correspond to radiation from the back. Let signs be associated with E and H, such that E pointing upward and downward denotes a positive and negative amplitude, respectively. While H pointing right and left denotes also a positive and negative amplitude, respectively (readily convertible into loop voltage signs). The four possibilities may be tabulated as follows.

	E	H	Source
a)	-	+	front
b)	+	-	front
c)	-	-	back
d)	+	+	back

It is evident from the table that E and H have opposite signs if the source is in front, while they have the same signs if the source is in back. It is not difficult to apply the same procedure to the second loop.

Thus it is readily seen why electrical noise can produce 180^{o} errors. If the signal-to-noise ratio is too low or the electronics is ineffective, electrical noise pulses of the wrong sign can overwhelm the electric field amplitude and make it appear, say, negative when it should be positive, and vice versa. Similar errors may be caused by unintentional phase shifts in the signal amplifiers.

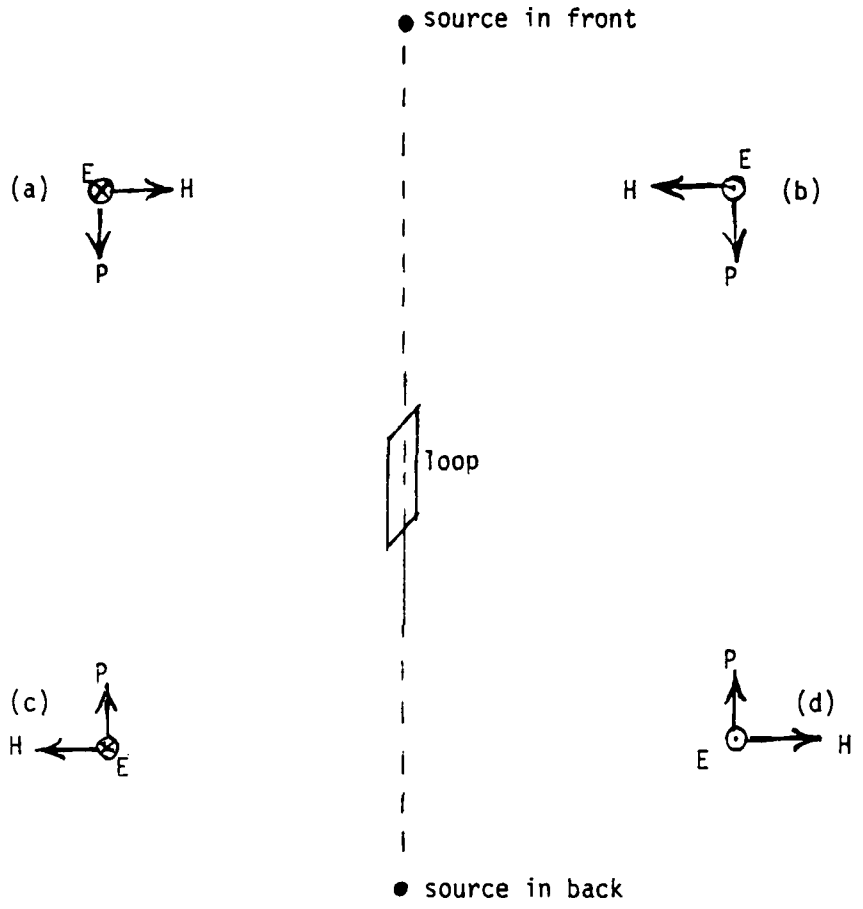

FIG. 6. Resolution of 180-degree ambiguity

2. Errors in Direction-Finding

In theoretical discussions it is usually assumed that the electromagnetic field is linearly polarized, implying that the source current flows in a straight line. The lightning channel, however, is not a straight line but generally follows a rather tortuous path with branches in all directions. Such a source current has many significant horizontal components. Consequently the assumption of linear polarization can result in rather large errors in direction determination.

(a) Slanted Lightning Channel Errors

Even if the current can be assumed to flow in a straight line, in general it is nonvertically oriented. If we are restricted to detection of two magnetic field components (parallel to the ground plane), the "slant" lightning channel, if it is at any significant altitude, plus its image in the conducting ground plane, will cause the crossed loop to determine an erroneous direction. That is, the magnetic vector at the crossed loop, instead of being perpendicular to the line of sight (as in Fig. 6) will have another direction and a different source direction (perpendicular to the observed magnetic vector) will be inferred.

This effect has been analyzed by Kalakowsky and Lewis (1966) and Uman et al (1980), but only with the crossed loop detector at the ground. This results in simplifications. The more general case where the detector is also at a non-negligible altitude (i.e. airborne) above a conducting ground plane does not appear to have been considered in the literature. Hence we present an appropriate analysis in Appendix A. In the following we discuss some key results and sample applications of the analysis.

The error in direction due to a slanted lightning channel may be expressed as (see Fig. A-1, App. A):

$$\text{Misdirection Angle} = \arctan \frac{G\, P_y/P_z}{1 + G\, P_x/P_z} \qquad (2)$$

where P_x, P_y, and P_z are the components of the lightning dipole radiator (P_x horizontal in direction of observer, P_y horizontal and transverse to this, P_z vertical), and where G is a geometrical factor

$$G = (H + Qh)/D \tag{3}$$

where D is the horizontal distance from the dipole to the detector, H is the altitude of the dipole, and h is the altitude of the aircraft, both above a conducting ground plane. Q is given by Eq. (16) of App. A, re-expressed here as follows:

$$Q = [(x_1^3 - x_2^3)\dot{P} + (x_1^2 - x_2^2)\ddot{P}/c]/[(x_1^3 + x_2^3)\dot{P} + (x_1^2 + x_2^2)\ddot{P}/c] \tag{4}$$

where $x_1 = [D^2 + (H-h)^2]^{-1/2}$, $x_2 = [D^2 + (H+h)^2]^{-1/2}$ and $\dot{P}$ and $\ddot{P}$ denote first and second time-derivatives of the moment P. Note that Q vanishes when the detector is on the ground plane (h=0) and G=H/D from (3) then leads to the simple result given by the cited papers.

As an example we assume that the lightning is at D=15 km from the aircraft and at height H=3 km. We also assume that the dipole is tilted at 45 degrees such that $P_y=P_z$ and $P_x=0$. If the aircraft is on the ground we have h=0 so that G=0.2. Then from (2) the misdirection angle is arc tan G = arc tan 0.2 = 11.3 degrees. Next assume the aircraft is at 3 km altitude (= h). We may evaluate Q from (4) if P(t) is known.

Or, we may assume that the dipole is a harmonic radiator of fixed frequency and use the alternative complex form (24) of App. A. Thus we obtain:

$$\text{Re } Q = 0 \quad \text{for} \quad h = 0 \tag{5}$$

$$\text{Re } Q \sim -\frac{(3 + 2k^2 D^2)\, H^2}{(1 + k^2 D^2)\, D^2} \quad \text{for } h = H \ll D \tag{6}$$

$$\text{Re } Q = -\frac{(0.91 + 0.88\, k^2 D^2)}{(1 + 0.59\, k^2 D^2)} \quad \text{for } h = H = D \tag{7}$$

(Re = real part)

where k is the wave number. Note from (5) - (7) that the correction factor Re Q for finite aircraft height (h) has negative values ranging from zero to about -3, for all values of kD. Here we are assuming D greater than H (distance from lightning greater than lightning height).

Now assume a frequency of 50 kHz (Stormscope central frequency). With the lightning at distance 15 km (=D), at height 3 km (=H), and with the aircraft at altitude 3 km (=h), we use (6) to obtain Re $Q \tilde{=} - .10$, a relatively small correction leading to G=0.18 as opposed to the h=0 value of 0.2. Hence the misdirection angle is nearly the same (under the assumed conditions) when the aircraft is at 3 km as when it is on the ground.

(b) Site Error

Another kind of error leading to errors in direction-finding by magnetic crossed loops is re-radiation (or scattering) of the incident magnetic field by nearby conducting surfaces (site error). When the crossed loop is mounted on an aircraft conducting surface this error can be important. We are unaware of any treatment of this effect for airborne application (although the work of Horner (e.g. 1954) is well known for treating site errors at the ground due to buried cables, hills, etc.). An analysis of this effect for airborne application is given in Appendix B. We believe that this analysis is original. Some key results and sample applications follow.

The misdirection error due to the reradiation from the aircraft skin depends on the geometry of the aircraft and the position where the detector is mounted.

In Appendix B we have assumed the magnetostatic limit (wavelength >> aircraft dimensions) and solved Laplace's equation to obtain the perturbation field. For an arbitrary angle of incident direction the longitudinal and transverse magnetic field components are enhanced by different factors giving rise to misdirection or site error.

Assume the detector is mounted on top of a fuselage, and that the fuselage has the shape of a long cylinder of circular cross-section.

Assume the incident direction is at 0^{o} if along the axis, and at 90^{o} if perpendicular to the axis. Then Table 1 (App. B) shows that the error is zero degrees if the incident direction is 0^{o} or 90^{o}, but increases to a

maximum of -19.5° angle error at an incident direction of 55°. This result is independent of the cylinder radius.

Now assume that the fuselage is modeled by a prolate spheroid of aspect ratio 0.1 (ratio of minor to major axes). This approximates an F-106 Delta Dart, for example. Table 3a (App. B) shows that a detector on the top at the center of the fuselage experiences a maximum angle error of -18.4° at incident direction 55°. If the detector is moved forward (or backward) to very near the nose or tail (Case y=0.99b in Table 3a) the angle error increases to -23.6° at incident direction 60°, and reaches -60° (that is the negative of the incident direction) on the nose or tail.

If the aspect ratio is 0.2 (more nearly characteristic of a C130 geometry which lies between 0.1 and 0.2), then Table 3b shows that the maximum error angle is -16.4° at incident direction 55°, if the detector is centered front to back. This error increases to -30.7° if the detector is nearly on the nose or tail, at incident direction 60°. Again the error is minus the incident direction on the nose or tail.

As the fuselage becomes thicker compared with its length the error becomes smaller at the central position, and larger at the far forward and aft positions. The model becomes a sphere when the aspect ratio is unity (Table 3d).

Appendix B presents formulas for the above errors. Also treated is the case of a cylinder of elliptic cross-section, which can be used to model the situation where the detector is on a symmetric wing or on a tailfin. When the detector is on the center of the flat part of the wing, away from edges, the error is negligible. However, if it were mounted on top of a thin body such as the edge of a tailfin the maximum error becomes very large.

(c) Ionospheric Reflection Error at Very Low Frequencies

When the lightning source is sufficiently far away the radiation can propagate by multiple paths. One is a ground wave which arrives first.

This is followed by the first ionospheric-reflected wave ("sky-wave") and then by many more echoes. The ground wave should be free of polarization changes, but this is not the case for the sky-wave. The largest error due to the sky-wave occurs when the sferic originates at a distance of about 300 km, leading to rotation of the magnetic vector and changes in the apparent bearing of the source from 10^{o} to 30^{o} (Horner, 1957, 1964). The error should diminish with decreasing distance, however, and will probably be negligible at distances of interest, under 200 km, because the ground wave becomes stronger at closer ranges. (At about 300 km, the ground-wave and sky-wave amplitudes are comparable.) One can also "gate" the initial part of the signal to discriminate against the sky-wave which is delayed in time (W. L. Taylor, private communication, 1980).

3. Range by Multiple Stations

To obtain the range of a lightning discharge, two crossed-loop bearing-detector stations may be used with triangulation. This requires (a) that the baseline of the system be of the same order as the range of the source (lightning discharge), and (b) that the direction of the source be different from that of the baseline. Otherwise small errors in reading the angle will result in large errors in the determination of the range.

The remedy in the case of ground-based stations is to use 3 stations at the vertices of an equilateral triangle, with sides (baselines) on the order of tens of kilometers. This arrangement allows redundant verification of the position determination by each pair of stations. On an airplane one may be restricted to a single station, and the range would have to be determined by a different means. Single-station range detection has proved to be a difficult problem. A number of solutions have been suggested (see subsection IV. B. on single-station range detectors).

4. Stormscope

A modern commercial version of the crossed loop, the Stormscope instrument presently available for airborne application (Ryan, 1977), uses a single crossed loop for the determination of the azimuthal direction (bearing) of lightning discharges with respect to the aircraft. The operating frequency band is centered on 50 kHz, that is, low frequency. Ranges of 40, 100, and 200 nautical miles may be selected. Lightning positions are displayed as dots on a CRT "scope". In the present version the dots do not move so as to reflect the change in position of the aircraft. Such dots cannot show the spatial extent of the source. Also, the manufacturer claims that Stormscope rejects signals from horizontal discharges. Hence some data from nonvertical discharges would be lost. The manufacturer claims a range accuracy of $\pm$10 percent, minimal errors from reradiation by nearby metal surfaces, and invulnerability to corona noise because of special signal processing techniques.

The Stormscope is of considerable interest because of its compact geometry and relatively low cost. Its accuracy and reliability are still in the process of being assessed.

The range is indicated by the radial distance of the dot from the center of the display. According to the manufacturer, the range of the lightning discharge is obtained by computer evaluation of signal strength, time to peak value, decay time, spectral content, and comparison of electric and magnetic field amplitudes. The details of the physical concept of this evaluation could not be obtained at the present time. Therefore, the accuracy of the range determination is still an open question.

5. Stormscope Tests

In-flight field tests of Stormscope were performed by the Air Force Flight Dynamics Laboratory in 1977 (Seymour and Baum, 1979; Baum and Seymour, 1980) with funding by the FAA. (See also Rozelle, 1979.) The instrument was installed near the leading edge of (and on the underside of) the right wing tip of a T-39B aircraft. This location was chosen to reduce spurious responses because the instrument is very sensitive to electrical noise generated within the aircraft.

The tests were performed near thunderstorms at Kennedy Space Center, in conjunction with on-board air weather radar (X-band), ground weather radar, and the ground-based LDAR system for locating lightning discharge sources. (LDAR is an elaborate time-of-arrival system discussed later.)

Some key results of the Stormscope tests are:

1) Some reasonable correlations are obtained of Stormscope dots with weather radar precipitation echoes, with some discrepancies.

2) Stormscope dots are *much* more dispersed both in range and azimuth than LDAR dots, although roughly in the same general area.

3) Isolated Stormscope dots sometimes appear in the fair-weather region roughly 180^{o} opposite the main activity. We believe these could be due to the 180^{o} sensing errors discussed above.

4) With respect to range, Stormscope tends to indicate activity more distant than LDAR. Moreover, Stormscope sometimes shows a "radial spread" or "spoke" effect, a radial distortion of dots apparently due to range errors.

In summary the authors (Baum and Seymour) feel that despite the apparent over-spread of its dots (which probably results from range and bearing errors), Stormscope provides a conservative warning of severe weather, i.e. larger avoidance areas than LDAR.

Spurious indications by Stormscope (high "false alarm rates") have also been observed in ground-based tests for mining applications (Johnson et al, 1980).

On the other hand, it should be noted that some private pilots have found Stormscope helpful in avoiding thunderstorms (R. Rozelle, R. Collins, personal communications,1980).

6. Gated Wide-Band Direction-Finding System

A recently-developed crossed-loop detector system, called the Lightning Location and Protection (LLP) system, operates with gated wide-band (GWB) electronics (Krider et al, 1976, 1980). This system is presently ground-based and is designed to locate exclusively cloud-to-ground return strokes, by triangulation using two or more well-separated stations. It rejects signals due to intracloud discharges, background noise, and return strokes lowering positive charge to ground. For an accepted signal the bearing error due to slant in the lightning channel can be reduced, to under 1^{o} according to NSSL tests by M. W. Maier (personal communication, 1980), by gating on the first few microseconds of the signal. This corresponds to radiation from the lowest 100 m of the return stroke channel. The misdirection is minimized because the source and the detector are both essentially on the ground plane (see "Slanted Lightning Channel"). The LLP system uses 1 kHz to 1 MHz as its operating frequency band. It is commercially available and has recently seen widespread ground-based deployment by the USDI Bureau of Land Management to detect forest fires (Krider et al, 1980). The LLP system can be used as close as 1 km from a return stroke channel (*M. A. Uman, personal communication*). A similar system has been reported by Bent (1979), using however 1 kHz to 100 MHz.

With respect to possible airborne application, a single-station version of the LLP system probably can be adapted to locate return strokes and display the data in a manner similar to Stormscope. The LLP system would as well as Stormscope be subject to site errors. These can be minimized by appropriate calibration.

7. Kohl's Multiple Loops

A system of multiple magnetic loops has been developed by Kohl (1966) for determining the direction of sources of RF signals including sferics. It is in essence a removal of the two-component limitation of the crossed loop antenna, and extension to a 3-component sensor by the addition of a third loop in the third direction. Airborne experiments have been sponsored by AFGL, and the system has been flown experimentally on a Canadian ASW patrol aircraft (D.A. Kohl, private communication, 1980). The system operates at 500 kHz and is capable of detecting a magnetic vector of arbitrary orientation, using appropriate electronics. It therefore has in principle a (vector detection) capability greater than that of a single pair of crossed loops. This implies for example that bearing errors due to slanted lightning channels can be eliminated.

B. RF Sferics Single-Station Range Detectors

It was mentioned earlier that single-station range detection is a difficult problem area. Some proposed solutions will be discussed in this section.

1. Stormscope

In our discussion of Stormscope we referred to its range indication. One would infer from the patent description (Ryan, 1977) that the range is obtained from assuming that the detected magnetic field intensity H is inversely proportional to the distance r. If one is sufficiently far from a radiating dipole (so that the induction term is negligible compared with the radiation term - see Eq. (9)) then H=K/r, where K is a constant proportional to the time-derivative of the current. If K were known and truly constant (all lightning discharges having the same di/dt), then the range would be simply given by K/H.

However, lightning discharges are highly variable and are distributed with respect to di/dt.* Data on parameters of lightning discharges are difficult to obtain. For cloud-to-ground strokes, data have been obtained by Berger. Some of this is tabulated by Golde (1977). The data for negative strokes may be fitted roughly by a log-normal distribution with standard deviation about 5 dB. The corresponding figure given by Pierce (1977b) is 7 dB for VLF emissions. This standard deviation, corresponding to factors of about 2 and 1/2 with respect to the median, would thus apply also to the range determinations. Hence variability alone would lead to both underestimates and overestimates in range by factors of 2.

An additional problem with using magnetic field intensities is site error. As shown in App. B, depending on the location of the instrument on the airplane, the apparent magnetic field intensity H can be enhanced by as much as a factor of 2. Under the r=K/H assumption, this would lead to underestimates of r by a factor of 2. The site effect can also cause diminutions of H, leading to overestimates of r.

*This may contribute to the Stormscope "spoke" effect (see p. 40).

2. Kohl's 500-kHz Sferics Range Detector

Following investigations by Norinder, Malan, and Horner of sferics radiation properties, Kohl (1969, and references cited therein) notes that at 500 kHz most of the radiation is not from the return stroke per se but rather from the breakdown processes associated with the lightning (e.g. predischarges). Using a simple omnidirectional electric antenna (wire), the pulse spectrum at 500 kHz is found to contain maximum pulse amplitudes essentially the same for all lightning bursts. Thus peak pulse measurements using spectrum analyzers can form the basis of a range determination when properly calibrated against radar echoes. The variation is monotonic with range and occurs from direct-path propagation losses (i.e., ground waves). The variation depends on the conductivity of the soil.

Empirically, one must detect pulses over several minutes to have a high probability of having detected the peak pulse(s). That is, large numbers of pulses (~500) must be detected. Also, large amounts of radar data are required to reduce the probable error. Kohl (1969) reports a standard range detection deviation of ± 2.6 km over all data ranging from 2-274 km. In a recent private communication he claims his range error to be under 10 percent in the range 25-200 miles. In addition, a rough fit to his data is given by amplitude proportional to $1/r^{1.1}$.

A difficulty of the calibration with respect to applicability to airborne use arises because a new calibration is initially required at any new location because of the changed ground conductivity characteristics.

Regarding the existence of an invariant maximum pulse height, Kohl says that there is (at 500 kHz) "an apparent maximum limit of the radiation energy at that frequency. The nature of the sources at the instant that the maximum occurs is unknown but it arises during the complicated electrical breakdown processes associated with lightning (the growth of the leader). This limit appears to be independent of major variations in return strokes."

3. Spectral Amplitude Ratio and Group Time Delay Difference

There is a possibility of using spectral amplitude ratios (SAR), employing two VLF frequencies and sharply-tuned receivers, for sferics range determination using propagation characteristics of the earth-ionosphere wave guide. Thus, for example, Schäfer et al (1980) use two frequencies, 5 kHz and 9 kHz and employ a propagation model to obtain a linear relation relating the spectral amplitude ratio SAR (ratio of voltage outputs at the two frequencies from a whip antenna) to range R: SAR=A+BR, where A and B are constants given by the model. They assume the far field and a perfectly conducting earth, plus the "first mode" approximation. Hence, the range R is obtained when SAR is measured. Use of SAR is also suggested by Pierce (1956).

Another parameter is also used based on the high dispersion characteristics of the waveguide in the range 3-10 kHz. This is the group delay time difference (GDD), which is defined from the phases of 3 equidistant frequency groups, at 5, 7, and 9 kHz. The GDD is formed from the propagation times of the groups at 6 and 8 kHz (5 to 7 and 7 to 9, respectively). From the theory of VLF propagation, assuming the first mode only yields GDD=KR so that R is determined when the GDD is measured. According to Pierce (1977a) the GDD parameter is presently preferred for estimating distance.

In the near field (less than 300 km range) the interference of several higher order modes in the propagation of VLF waves gives rise to ambiguities in the data. Hence SAR and GDD data are used in conjunction. The minimum range such that the higher-order mode interference may be neglected is about 300 km.

It may be possible to adapt this method to airborne use (H. Volland, private communication, 1980). However, the method seems to require large amounts of statistical data, which is time-consuming. Hence adaptation would require careful consideration.

4. Electric-Field Range Detection

Other possible range-detection methods can make use of the dependence on distance of electric-field amplitude (E) or the ratio of magnetic-to-electric field amplitudes (H/E). In order to clarify the relationship of field amplitude to source strength and distance, we model the source by an oscillating dipole and consider the equations for the electric and magnetic fields:

$$E(r,t) = M(t)/4\pi\epsilon r^3 + dM(t)/dt/4\pi\epsilon c r^2 + d^2M(t)/dt^2/4\pi\epsilon c^2 r \quad (8)$$

and

$$H(r,t) = \mu dM(t)/dt/4\pi r^2 + \mu d^2M(t)/dt^2/4\pi c r \quad (9)$$

Here we denote:

$E(r,t)$, $H(r,t)$ = electric and magnetic field amplitudes
$M(t)$ = dipole moment (charge x length)
r = distance of receiving station from centerpoint of dipole
c = velocity of light
ϵ = electric permittivity of air
μ = magnetic permeability of air

These equations (which can be found in equivalent form in many textbooks (e.g. Pierce, 1977a)) are based on the following assumptions: The radiating source is a dipole of length ℓ with its axis vertical. Its length and orientation are constant in time, and the current is constant along its length. The distance r is large compared with ℓ. (Lightning discharges do not generally fulfill all of these requirements.)

The equations are valid for a receiving station at the ground where the electric field has only one component, perpendicular to the ground plane, while the magnetic field has one (azimuthal) component parallel to

the ground plane. Therefore it is possible to express E and H as scalar functions. For an observer in space above the ground plane (e.g. on an airplane) $\vec{E}$ and $\vec{H}$ are three-dimensional vectors, and Eqs. (8) and (9) must be supplemented each by two more equations for the other two vector components.

In Eq. (8) the $1/r^3$ term is designated as the "electrostatic field" term, while in (8) and (9) the $1/r^2$ and $1/r$ terms are designated as the "induction field" and "radiation field" terms, respectively. The $1/r^3$ term dominates in the "near zone," while the $1/r$ terms dominate in the "far zone."

The values of the scalars (or vectors) E and H depend not only on range r but also on the time-derivatives of the dipole moment, M, dM/dt and d^2M/dt^2. If the electric (or magnetic) field amplitude is to be used as an indicator of range, it must be assumed that M and its time-derivatives are the same - or approximately the same - for all lightning discharges detected. This is not the case, however, and variability among different lightning discharges can amount to an order of magnitude or more. A nearby weak discharge may thus produce a field strength of magnitude similar to that of a distant strong discharge.

Therefore a dispersion or spread may be expected in data representing field amplitude versus distance. The data in Fig. 7, representing electric field amplitude versus distance (Kasemir, 1962) illustrates such a spread. The electric field and distance are given by the ordinate and abscissa, respectively. The field was measured with a capacitive-loaded antenna with a time constant of 5 sec. The distance was obtained by triangulation from visual observations at two stations separated by a baseline 23.5 km in length.

We may read this figure in two ways. One way is to determine the spread in field values at a given distance, (e.g. 30 V/m to 230 V/m at 20 km, and 3.2 V/m to 10 V/m at 70 km). We may on the other hand determine the spread in distance values at a given field value, e.g. 15 km to 23 km at 200 V/m, and 66 km to 90 km at 4 V/m. The first set of data is more nearly representative of the "near zone" given by the first term on the right-hand

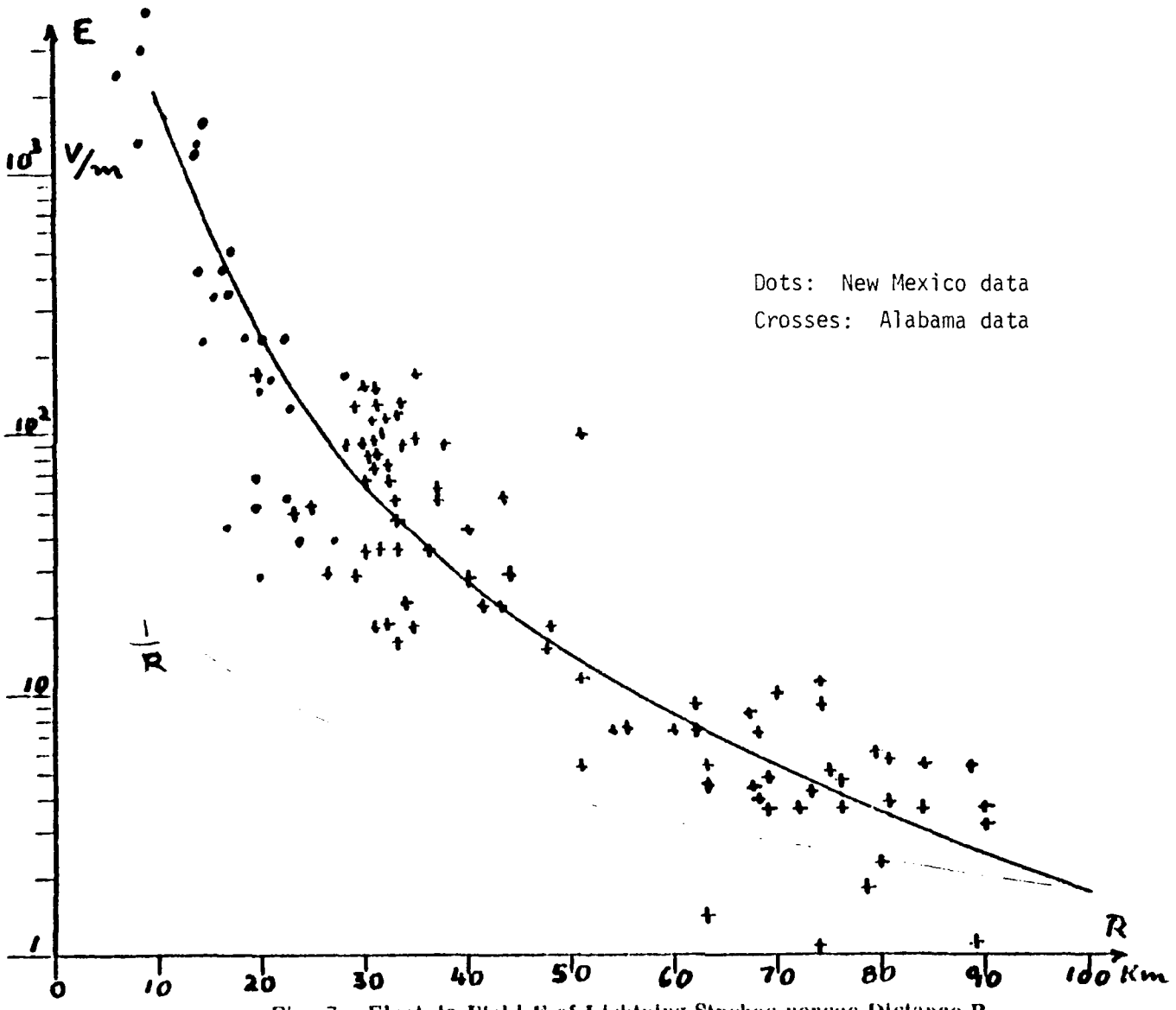

Fig. 7. Electric Field E of Lightning Strokes versus Distance R

side of (8), and has a range spread of ±21% about its central value of 19 km. The second set of data is more nearly representative of the "far zone" given by the third term on the right-hand side of (8), and has a range spread of ±19% about its central value of 78 km. It appears from these and other samples that the relative error is about ±20% of the range, independent of the range itself. This gives a rough idea of the error to be expected if the electric field amplitude is used for range detection. The solid curve in Fig. 7 corresponds to a $1/r^3$ variation. For comparison, an inverse-distance law (dashed curve) is also shown, normalized to the solid curve at 100 km and 2 V/m. It is clear from these results that the $1/r^3$ curve fits the data quite well almost to 100 km. However, the dashed curve indicates that a $1/r$ variation better represents the data beyond about 80 km. It is suggested that a fit to the data may be more effective as well as physically more nearly correct using 3 terms ($1/r^3$, $1/r^2$ and $1/r$) corresponding to Eq. (8).

Range detection based on the $1/r^3$ assumption has also been investigated by Ruhnke (1962). Both his results and data of the same type obtained earlier by Pierce (1955) appear to show a considerably greater spread than that indicated by Fig. 7.

5. Range Detection by Flash Counters

A related problem arises in the error determination in the measurement of the lightning density (flashes per square kilometer) by lightning flash counters (Horner, 1960). That is, one records the discharges within a defined radius from the instrument. A wide-band low-frequency receiver is used, responding to sferics electric fields having amplitudes greater than a certain threshold level. The problem is then to determine the distance that corresponds to this threshold value.

It was discovered that the accuracy of the radius determination was poor due to the great variability of the source strength. However, by suitable statistical treatment of large amounts of data, Horner (1960) established an effective range by comparisons between counter records and observations by visual and aural techniques.

In addition, there is a strong influence on the received signal strength by the differences in wave propagation characteristics during day and night. This effect is usually ignored by reports on testing of range indicators based on the amplitude of lightning-generated electromagnetic pulses. Tests for airborne applications of these techniques should include both day and night data.

6. Range Detection by H/E Ratio

To eliminate the influence of the source strength represented by the dipole moment and its time-derivatives in (8) and (9) Ruhnke (1971a) suggested the use of the ratio of the magnetic to electric field amplitudes H/E. In the near zone this ratio increases linearly with r because of the $1/r^3$ dependence of E and the $1/r^2$ dependence of H. In the far zone the ratio becomes constant since E and H are both proportional to 1/r. The problem here is that in the near zone, where there is a variation of H/E with r, E is proportional to M while H is proportional to dM/dt. Thus, for range detection it must be assumed that (dM/dt)/M is constant for all discharges. This implies that M(t) must be exponential in time. As yet there is no evidence that this holds even approximately. However, it would seem worthwhile to pursue this approach. One would have to take into account also the day and night differences, or assume that these are eliminated by the same method.

C. Special Systems

In this section we consider some examples of special systems for direction-finding and location of sferics sources. Time-of-arrival (TOA) systems, an interferometer system, and an electrograph system are included.

1. Time-of-Arrival (TOA) Systems

Two examples of Time-of-Arrival (TOA) systems for detecting sferics from discharges in electrified clouds are

(a) LDAR (Lightning Detection and Ranging) (Poehler and Lennon, 1978 and 1979)

(b) Taylor's Lightning Mapping System (Taylor, 1978)

The two systems operate similarly in that all the antennas in an array receive pulse signals radiated from the same discharge source located at a point in space at a given time. Using the differences in the times of arrival of the pulse at the individual antennas, an analysis may be performed yielding the coordinates of the source (angles of azimuth and elevation, plus range with a sufficient number of antennas).

The analysis generally depends on the fact that, for any one pair of antennas and a given difference in TOA of the pulses to them, the source must be located somewhere on a unique hyperboloid of revolution with the two antenna positions at the focii. For another pair of antennas in the group detecting the same pulse, there is another hyperboloid of revolution. The intersection of the two hyperboloids gives a curve in space on which the source must lie. A third hyperboloid, associated with a third pair of antennas, intersecting with the latter curve serves to locate the source position.

The accuracy of source location in space should be high if the source is within a range comparable to the effective baseline dimension (i.e., average baseline dimension for a group of several antennas). If the source is far away compared with the effective baseline dimension, the range is

difficult if not impossible to determine, but the direction (azimuth and elevation angles) is determinable. In this limit the hyperboloids become cones, and the intersections become straight lines. It should be noted that using two or more small-baseline groups of antennas with the groups separated by large distances increases the effective baseline dimension. Thus, the LDAR system typically uses 4 stations in a Y-configuration with an effective baseline of 10-20 km, so that the range of sources within 10-20 km of the center can be determined accurately. The Taylor system, on the other hand, uses two groups of antennas, separated by about 20 km, with baselines of about 14 m within each group.

Both of the above TOA systems operate in the approximate frequency range 20-80 MHz. A small amount of radiation from return strokes (< 10 MHz) is detected. Both systems also depend on fast rise times of the signals to mark the times of arrival. Hence weak signals and slow rises are rejected.

Two kinds of time resolution are involved:

1) The time resolution for a given pulse, which controls the accuracy of the angle determination, and
2) The time window for resolving individual pulses.

The time window for resolving individual pulses appears to be about 50ns for Taylor's system, and about 100μs for LDAR. These intervals are dictated by the systems used for processing the signals. The TOA systems can typically detect 50-100 discharges accompanying a ground strike, occurring within milliseconds of the strike. Reception rate (e.g. 25,000/s) is independent of the time window for receiving individual pulses (W. L. Taylor, private communication, 1980).

With respect to the time resolution for a given pulse, and its angle determination, the angular error ($\Delta\theta$) is related to the time resolution (Δt) approximately by

$$\Delta\theta^{\circ} \sim 60\frac{c\Delta t}{d} \qquad (10)$$

where c is the speed of light, and d is the baseline dimension. One method of estimating Δt is to perform laboratory tests on differences in times of

arrival, if the baseline is small enough; this involves careful adjustment of band-pass, time-delays, and thresholds. Another method is to use simply a number of the order of the inverse of the frequency bandwidth of the system. The use of different definitions may explain differences in estimates of accuracy. In any event, the above formula indicates that the LDAR system with its long baseline (d) has a potentially high location accuracy. However, difficulties may arise because of the long baseline. If the time between emissions of separate VHF pulses in the clouds is of the order of or less than the pulse propagation time between stations (30-50μs) the system may become confused.

Some individual characteristics and airborne applicability of the two TOA systems are described next.

(a) LDAR System

The antennas of the LDAR system are separated by tens of kilometers and are all in the same horizontal (ground) plane. This means that the source x-y position determination is relatively precise when the source is (well isolated in time and) within a baseline dimension of the array. Otherwise, only the azimuth can be precise. Because of the planar configuration, elevation is inaccurate at low values (e.g., heights below 300 m). A hyperbolic direction-finding system with high accuracy and much larger baselines was developed earlier by Lewis et al (1962).

The extremely long LDAR baseline dimension makes it obviously inapplicable as an airborne system. Nevertheless, this instrument has its value for testing airborne systems (e.g., Stormscope versus LDAR tests), and it can also potentially be useful for communicating lightning activity data to pilots from the ground.

(b) Taylor's Lightning Mapping System

As opposed to using arrays of antennas in the ground plane as in LDAR, Taylor's group consists of two pairs of antennas, one with a horizontal baseline, and the other with a vertical baseline. The horizontal-baseline pair is used for azimuth alone, and the vertical-baseline pair is used for

elevation alone. The baseline of this group is of the order of 10 m (as opposed to the 10-km scale of the LDAR group). Thus, its output is azimuth and elevation (a direction line). Taylor uses two such groups, separated on the order of 10 km, plus triangulation to determine range.

The relatively small baseline of the Taylor group seems more applicable to airborne use than the LDAR. However, the reduction of the baseline to the order of 10 m or less (suitable for aircraft) can result in large angular errors. For example, if we use Eq. (10) with d=3.6 m, and $\Delta t \sim (60\ \text{MHz})^{-1} \sim 1.7\times10^{-8}$ sec from bandwidth considerations, we obtain $\Delta\theta \approx 85^{\circ}$. This result suggests that high precision may be difficult to obtain with TOA-type airborne systems. However, the prediction of errors is apparently not as straightforward as implied in the foregoing. In this connection, Taylor (private communication, 1980) states the following:

"Bandwidth considerations for obtaining Δt are totally irrelevant for Taylor's system since the difference in time of arrival at each pair of antennas is obtained from the initial rise of the pulse waveform. Laboratory tests showed Δt could be measured to <0.5ns (no shorter interval was attempted). Field tests using the LDAR calibration pulse transmitter atop the VAB (Vehicle Assembly Building) at KSC and using an airborne pulse transmitter on a NASA aircraft for Oklahoma calibrations indicated the azimuth and elevation angles were determined to $<0.5^{\circ}$ error, thus showing that Δt was obtained in an operational mode to <0.4ns. For d=1 m in Eq. (10) we therefore have $\Delta\theta=7.2^{\circ}$. For d=3.6 m, very reasonable for aircraft installation, we have $\Delta\theta=2^{\circ}$."

2. Interferometer System

This instrument has been used in radio-astronomy to accurately locate extraterrestrial sources of ratio emission. It has been adapted to lightning location by Warwick and Hayenga (Warwick et al, 1979; Hayenga, 1979). In the present version, a 10-percent-relative-bandwidth receiver receives VHF

radiation at 34.3 MHz emitted by breakdown processes occurring at the tip of a lightning channel. The frequency f is one of several adjustable parameters, to be defined later. The relative phases of the signals arriving at a pair of omnidirectional antennas contain the desired information regarding the direction of arrival of the signals. The antennas are separated in the current version by a baseline d equal to twice the wavelength λ. (In the present version, $d=17.4m=2\lambda$). The accuracy of determination of the source direction depends on the accuracy with which the relative phase can be determined. The determination is simplified by mixing the outputs of the antennas with local oscillator signals offset in frequency by an amount f_o (typically 200 kHz) much lower than f. The signals are then multiplied with each other, producing an interference pattern with a sinusoidal modulation having the frequency f_o. The phase of the modulation, which can be determined accurately from successive zero-crossing times of the signal, is directly related to the relative phase of the original-frequency signals arriving at the two antennas.

The inherent high accuracy of source-direction determination by this method is limited in part, however, by the observation time τ (time of averaging) of a given train of waves. The method assumes that the train of waves is sufficiently long to produce an interference pattern, and that the radiation comes from a single source of small size during the time of observation. If the radiation comes from multiple sources the direction determination may be in error. Hence the received radiation is averaged over a sufficiently short time interval to minimize the possibility of confusion with other sources. In the present design this time interval τ is of the order of 1-2μs. Thus, pulses separated by 2μs or more and their associated sources can be resolved, and pulses lasting much longer than 2μs can be sampled every 2μs to determine motion during the pulse.

From the above phase shift, one infers the polar angle of the source with respect to the baseline direction. This determines one angle. Crossed baselines (two elements on each line) give the vector direction (both azimuth and elevation). Using two such groups widely separated can yield the source position by triangulation. The above technique was designed (by Warwick and Hayenga) for detecting the steps of a lightning stepped leader.

The accuracy of source-angle determination (azimuth and elevation) depends on four parameters of the system: wavelength λ, baseline d, bandwidth B, and integrating or averaging time τ. In degrees, the angle error may be expressed (aside from a trigonometric factor) as

$$\Delta\theta \sim \frac{90}{2\pi}\frac{\lambda}{d}\frac{1}{\sqrt{2B\tau}} \tag{11}$$

Hence, for 34.3 MHz and $d=2\lambda=17.4$ m, for B=4 MHz (roughly 10 percent of the frequency), and for $\tau\sim 5/B\sim 10^{-6}$s, we obtain the error:

$$\Delta\theta \sim 2.3^{o}$$

Another convenient design formula is obtained from (11) by solving for the frequency f, with B defined as 0.1f, namely,

$$f^{3/2} \sim \frac{90}{2\pi\,\Delta\theta}\frac{c}{d}\frac{1}{\sqrt{0.2\tau}} \tag{12}$$

where c is the velocity of light.

In a possible application to airborne use, d would decrease. Let d=3.6 m, as before. The frequency can be increased to 167 MHz to keep the same ratio of λ/d. The bandwidth B would increase to about 16.7 MHz, while the time τ can remain the same. Thus, Eq. (11) would yield a smaller $\Delta\theta$ because of the larger value of $\sqrt{B}$, yielding an even higher accuracy (by a factor of about 2).

The drawback to the above set of parameters is that the frequency 167 MHz would contain considerably less lightning radiation energy. The lowest frequency one may use in Eq. (11), with d and τ fixed, such that $\Delta\theta$ is no larger than one degree, is 4.6 MHz, or λ=65 m. This frequency is sufficiently low to contain significant energy. However, there may be considerable extraneous broadcast noise in this band.

The interferometer and TOA systems both seem to have considerable freedom in the choices of the parameters. They seem readily adaptable to airborne use. The possibility of range determination in addition to azimuth and elevation should be looked into.

With two stations, e.g. one on each wing of a large airplane, range may be determined by triangulation. The ranging accuracy depends on the angular accuracy of the individual stations. For an interferometer system the possible angular accuracy increases with the (square root of the) integration time τ. While use of as-small-as-possible values of τ (e.g. 2μs) would allow finer details of discharges to be detected, the resulting large amounts of data would be more appropriate for a ground-based research system than for an airborne lightning warning system. An interferometer system with increased τ (more accuracy, less detail) is relatively easy to implement and more suitable to airborne application (C. O. Hayenga, personal communication, 1980). As an example, it is suggested by J. W. Warwick (personal communication, 1980) that (with two crossed-base-line stations on a large airplane) using τ=75 ms at 600 MHz can yield a relative range accuracy of 33% at 200 km.

3. Electrograph and Crossed-Adcock Antennas

A lightning warning ("Electrograph") system operating at high frequencies, in the 900 MHz region, has been proposed by E. A. Lewis and his coworkers. A directional parabolic antenna scans both azimuth and elevation to detect radio noise pulses originating in small-scale electrical discharges (pre-discharges) preceding overt lightning flashes (Harvey and Lewis, 1972). In this sense the system is similar to the lightning-mapping TOA and interferometer systems.

A sferics system for lightning bearing detection in the broadcast band of frequencies (0.5 to 1.5 MHz) was developed by Stergis and Doyle (1959). Two Adcock antennas placed at 90^{o} to one another were selected over crossed loops because of the Adcock's lower sensitivity to polarization errors (due to down-coming sky-waves). Tests of crossed loops showed that 20^{o} to 30^{o} bearing errors were not uncommon. The accuracy claimed is about 5^{o}, with a potential reduction to 2^{o}.

With respect to possible airborne applications, the Electrograph is being designed for this purpose (R. B. Harvey, personal communication). It is uncertain whether the Adcock system can be made sufficiently compact. Also, the Adcock system may be as susceptible as crossed loops to aircraft site errors. These questions need investigation.

V. OPTICAL BEARING DETECTORS

Flash location by using the optical signals from lightning has some similarities to the sferics methods discussed in Sec. IV. For example, Kidder (1973) has described a South African system employing several cameras to give bearings, and subsequent triangulation to locate the discharge (Pierce, 1977b). Silicon photodiode systems have been used on a satellite for detection of lightning from space (Edgar, 1979; Edgar and Turman, 1980; Turman and Edgar, 1980).

An optical system for detection and recording of lightning on the ground, from aircraft and from space (the Orbiter) is under development by Vonnegut and his co-workers (Griffiths and Vonnegut, 1975; Vonnegut and Passarelli, 1978; Vonnegut et al, 1980). Their system consists of a photocell and a super-8 sound motion picture camera, designed to be hand-held.

Both the Vonnegut and the Edgar-Turman systems can detect lightning in clouds illuminated by direct sunlight even when the lightning cannot be seen by the human eye. Daylight interference is also avoidable to some extent by use of a filter for the H-alpha line which is much stronger in lightning than in daylight.

Thus far the optical systems available are suitable for picking up signals from the direction pointed to by the operator; they are not automatic direction-finders although various concepts for automatic systems are presently under consideration (B. C. Edgar, personal communication, 1980). Some comparisons of bearing detection of lightning between an optical sensor and a Stormscope sferics detector are presently being planned in terms of a ground-based study (O. H. Vaughan, personal communication).

With respect to range detection, a limitation of an optical system is the line of sight. Hence such a system would probably involve short-range triangulation.

With respect to bearing errors, in principle there should be none for vertical lightning channels. However, there is generally significant horizontal branching, and many lightning channels are approximately horizontal. These can represent broad sources, leading to large bearing errors. Another source-broadening effect occurs even if the channel is vertical. Namely, the

light emitted by the lightning can undergo nearly isotropic scattering with little attenuation within the same cloud or by nearby clouds, so that the light source as seen by the detector can be broad in extent. Thus, large regions of a cloud bank can be diffusely illuminated and subtend a large angle at the detector because of the light scattering (the whole cloud bank "lights up"). For example, a 10-km-wide cloud, brightly illuminated from lightning within and at a distance of 50 km constitutes a source subtending an angle 11.4^{o} at the detector. Thus the bearing error can be $\pm 5.7^{o}$.

In addition, the attenuation may become serious if the line of sight passes through a large thickness of cloud material, e.g. parallel to a frontal system.

These questions need to be considered in designing an optical lightning warning system.

Some possible constructions of optical detectors are suggested by the sketches in Fig. 8. The sketches labelled (a) in the figure use the dependence of photocell output on the angle of incidence of the incoming light (e.g. a cosine law). The detectors on the 4 side-surfaces of the cube or on the 8 surfaces of the cross (E. P. Krider, personal communication) will have different outputs in general dependent on the angle of the incident illumination. These outputs can be compared and analyzed to infer the correct direction.

The sketch labelled (b) is a rotating slit and mirror, using a single photocell. The sketches labelled (c) use a "fish-eye" lens or a parabolic mirror to direct incoming light to one of a large number of photodiodes arranged in a circle.

The dimensions of the above systems are very small, only of the order of an inch.

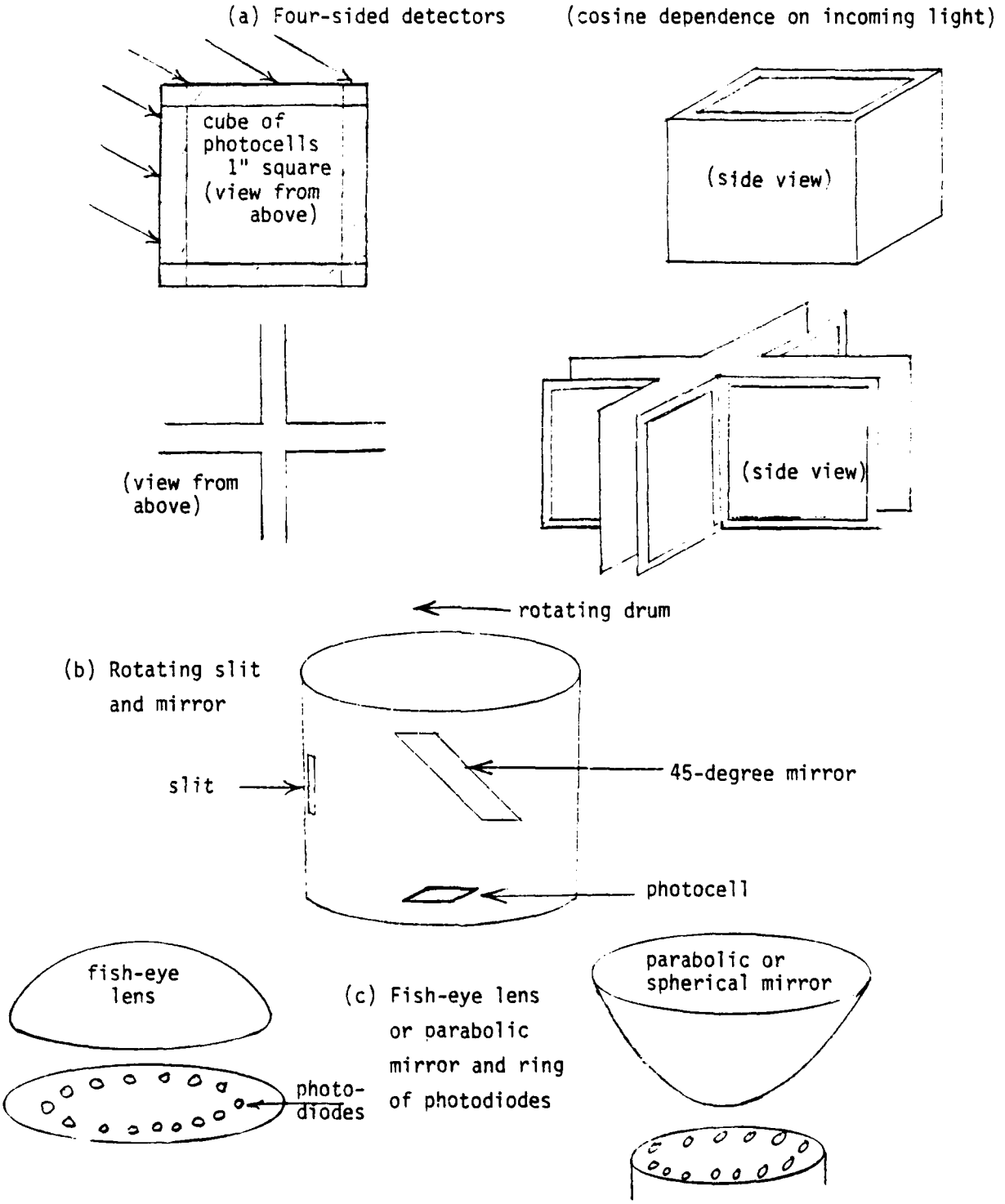

FIG. 8. Optical Detectors

VI. METEOROLOGICAL INSTRUMENTATION

Two airborne meteorological instruments of interest in lightning warning systems are the familiar airborne weather radar and a temperature sensor.

We consider first the temperature sensor which is of interest because the likelihood of encountering high electric fields and of triggering lightning by an aircraft is greater in some temperature regions than others (see Sec. II on triggered lightning and statistical evaluations). Typical airborne instruments for measuring temperature are a platinum wire and a reverse-flow temperature probe (Musil and Prodan, 1980).

A. Radar and Masking Effect

The airborne weather radar operates by reflecting (scattering) microwaves from precipitation-size cloud particles. It can detect precipitation areas over a range of perhaps 200 km. Although this system is widely used, care is required in interpreting the observed echoes. For example, reflection from a nearby heavy rain shower in front of a more distant severe storm can mask the severe storm behind, and lead to an erroneous interpretation that the storm is weak. This attenuating factor depends on frequency. Therefore, the design of the system requires care. There is less attenuation with longer wavelengths but then the antenna must be larger to keep the beam narrow. The standard wavelengths used are as follows (Battan, 1973):

Band	Wavelength (cm)
K	1
X	3
C	6
S	10
L	20

The S and L band radars are more penetrating than the C, X or K. However, they are generally too large for airborne use and are therefore ground-based. The S and L bands would not be subject to masking, but would only see large drops and hail, and would therefore miss light showers, particularly at a distance. The C-band is relatively old and has seen airborne use, but is being replaced by X-band units which are lighter and less expensive. Although X-band radar will see light precipitation and cloud particles down to about 100 micrometer in diameter, it is subject to the masking problem. Hence, an airborne radar system is a compromise between range capability and reflectivity capability.

The power intercepted by a radar antenna due to back-scattered radiation by particles of linear dimension small compared with the wavelength is proportional to the 2nd power of the inverse wavelength (Battan, 1973). With respect to the choice of radar wavelengths, we quote Mason (1971): "However, the increased absorption and attenuation of the incident and scattered energy at very short wavelengths may more than compensate for the higher reflectivity and seriously restrict the maximum range, and again a compromise has to be effected. The radar sets in general use (ground-based) work on either 10-cm or 3-cm wavelengths, 10 cm being essential if it is desired to penetrate heavy rain. Several people have suggested that a wavelength of 5.6 cm would be the most suitable for the study of precipitation, especially snow. A radar working on 5.6 cm would be roughly 10 dB more sensitive than an otherwise similar equipment working on 10 cm; but for a path of 100 miles through rain of intensity 10 mm/h, the greater attenuation on 5.6 cm would just offset this gain."

Some modern airborne radar units are digitally compensated for distance, and have 3 received-power threshold settings which are adjusted for nominal rainfall rates of weak, moderate and severe (C. B. Kitchens, personal communication, 1980).

Another type of radar is doppler radar that detects the velocity of motion of the scatterers. It potentially would be useful for detecting turbulence and strong updrafts and downdrafts. However, this is not contemplated for airborne use because it would be prohibitively expensive if it were intended solely for severe weather avoidance.

B. Lightning and Radar Echoes

Radar echo characteristics have been related to lightning by Fitzgerald (1978). Cloud-to-ground lightning is most likely to occur near the edge of the radar precipitation cores and in heavy rain sheets. In cold clouds "it is believed that dBZ values of 25 or 30 represent probable threshold values for initial cloud-to-ground lightning activity.... In the warm cloud case, the scanty evidence available suggests 35 to 40 dBZ as a more likely radar threshold."

Thick anvils (overhangs of thickness greater than 5000 feet) are likely to produce occasional but intense cloud-to-ground strokes, although they may extend a number of miles from the main precipitation cores. In some cases one or two isolated intense strokes may occur from the anvil when the storm appears to be dissipating. These anvils are difficult to detect with radar, "having only weak or no radar return depending on the individual radar system characteristics." They probably require X or C band units (at close range) for detection.

Fitzgerald suggests that data on time history of echo intensity and top height of moving storms are particularly significant for radar lightning warning, and "that it will be easier to decide if new cellular activity is likely to produce lightning than it will be to determine if additional lightning will occur from the older dissipating regions of a storm.... Nearly all convective tops reaching -40^{o}C and 50 dBZ echoes will produce some cloud-ground lightning."

VII. SUMMARY AND RECOMMENDATIONS

We have considered a number of instruments for possible airborne lightning warning systems. All have advantages and disadvantages. Some are well known and others poorly known.

In Table 1 we assign some tentative ratings to the various instruments considered. They are rated according to the following categories (acronym column headings):

AVAI = availability

SINT = simplicity of interpretation of data

SCON = simplicity of construction (essentially equivalent to cost)

SMAI = simplicity of maintenance

SCAL = simplicity of calibration

EXTT = extent tested (especially on aircraft)

PACC = potential accuracy

VERS = versatility (possible use for both near and distant warning, or for both range and bearing)

INSE = insusceptibility to errors (e.g. site errors) or to disturbances associated with the environment (e.g. rain)

The judgments are given in terms of letters:

L = low

M = medium

H = high

HH = very high

U = unknown

Asterisk (*) = in the present state of development - can be improved.

The instruments are segregated into 5 groups, arranged vertically in the table:

1. Field detectors
2. Sferics bearing detectors
3. Sferics range detectors
4. Optical bearing detectors (one-member group)
5. Airborne radar (one-member group)

A. Individual Assessments

(1) Among the field detectors we make the following comments.

Field mill: High in all categories except that they must be constructed, and construction is not simple.

Radioactive probe: Similar to field mill, but construction is much simpler. However, maintenance is not simple and some errors are possible.

Corona point: Extremely simple to construct and maintain, and not susceptible to errors. Interpretation may not be simple.

(2) Among the sferics bearing detectors we make the following comments.

Crossed loops: Available and relatively simple to construct and maintain. Susceptible to site errors, requiring careful calibration. Narrowband system tested with inconsistent results. Potential accuracy lower than that of gated wide-band system for detecting return strokes.

Kohl multiple loops: Must be constructed. Not extensively tested. Otherwise similar to crossed loop except that potential accuracy may be higher in detecting nonvertical lightning.

TOA and interferometer: Must be constructed. Mostly unknown properties except that potential accuracy may be high.

(3) Among the sferics range detectors, none have as yet high accuracy. We make the following comments.

Crossed loops: Comments similar to those on crossed-loop bearing detector. In addition, low potential accuracy and susceptibility to errors due to lightning variability may be difficult to improve.

Kohl 500 kHz: May be simple to construct, and promising, but largely unknown characteristics.

SAR-GDD: Available, simple to maintain, and tested to some extent. Otherwise not known.

E-amplitude: Available, versatile, and simple to interpret, construct and maintain. Extensively tested, but usually the time difference between lightning and thunder has been used to determine distance, and this is not accurate.

H/E ratio: Must be constructed, but simple to construct and maintain. Accuracy and error susceptibility unknown.

(4) Regarding optical detectors and airborne radar, we make the following comments.

Optical bearing: Simple to construct, maintain, calibrate and interpret. Must be constructed. Not versatile. Subject to reflection (scattering) errors due to surrounding clouds.

Airborne radar: Available and extensively tested. May be difficult to interpret because of possible masking effects. Cannot positively identify regions of electrical activity but valuable as an adjunct to any of the above systems.

B. Recommendations

We believe that many of these instruments have virtues worthy of consideration for airborne warning and avoidance systems. However, they require careful testing and evaluation. Many possible combinations of different types of instrumentation may be effective, for example, field and optical detectors in addition to radar. Also versatility of field detectors with respect to both near and distant warnings should be considered, as well as range detection with multiple bearing detectors.

Analyses performed in this report should be helpful in recognizing errors and in suggesting improvements.

Table 1. Characteristics of Instruments

	AVAI	SINT	SCON	SMAI	SCAL	EXTT	PACC	VERS	INSE
1. Field									
Field Mill	L	M*	L	H	H	H	H	H	H
Radioact. Probe	L	M*	H	L*	H	H	H	H	M
Corona Point	L	L*	HH	HH	M*	M	U	H	HH
2. Sf. Bearing									
Crossed Loops	H	M*	H	H	L*	H	L	M	L*
Kohl Multiple Loop	L	M*	H	H	M*	L	H	M	L*
TOA	L	L	U	U	U	U	H	M	U
Interferometer	L	L	U	U	U	U	H	M	U
3. Sf. Range									
Crossed Loops	H	M	H	H	L	H	L	M	L
Kohl 500 kHz	L	U	H	M	L	M	U	U	U
SAR-GDD	H	M	M	H	L	H	M	U	U
E-amplitude ($1/r^3$)	H[1]	H	H	H	M	M	L	H[2]	M
H/E ratio	L	M[3]	H	H	L	L	U	U	U
4. Optical Bearing	L	H	H	H	H	M	M	L	L
5. Airborne Radar	H	M[4]	L	M	M	H	U	M	U

[1] Lightning counter available in near-range form, not far range. Can be extended to 1/r variation.

[2] Slow antenna.

[3] Near-range only.

[4] May be difficult to interpret when masking occurs.

* In the present state of development - can be improved.

Notes: Electrograph and crossed-Adcock antennas not included: characteristics uncertain. LDAR not suitable.

Crossed-loop assessments here refer to narrow-band systems. A gated wide-band system applied to return strokes should be more accurate for bearing detection.

APPENDIX A

Polarization Errors in Lightning Direction Finding by Magnetic Crossed Loops: "Misdirection" Due to Nonvertical Orientation of the Lightning Channel

In this section we consider the error in magnetic direction finding due to the effect of nonvertical orientation of a radiating lightning channel, modeled by a radiating tilted dipole. The error in direction finding derived analytically here (to our knowledge not published previously) is that due to the tilt of the source dipole, where both source and observer are above a conducting ground plane. The magnetic crossed-loop detector is considered to be otherwise perfect (no perturbations due to the aircraft, etc.). The "misdirection" due to induced skin currents of the aircraft (siting errors) is treated in Appendix B.*

Referring to Fig. A-1, consider the detector to be at altitude h above the ground plane. (The loop is, of course, mounted on an aircraft, but the perturbing influence of the aircraft is ignored for the present.) The lightning radiation source is represented by a dipole of vector dipole moment $\vec{P}$, located at altitude H above the ground plane. Define a Cartesian coordinate system, wherein the ground plane is represented by the x-y plane, and the dipole is centered on the z-axis at a vertical height z=H above the ground plane. The detector is located in the x-z plane, at a height z=h above the ground plane, and at horizontal distance x=D from the z-axis (for y=0). Thus, the coordinates of the source and detector in this system are (0, 0, H) and (D, 0, h), respectively. Let R_1 denote the distance from the dipole to the detector, and let R_2 denote similarly the distance from the dipole image (at depth H below the ground plane) to the same detector. Then R_1 and R_2 are given by $R_1^2=D^2+(H-h)^2$ and $R_2^2=D^2+(H+h)^2$. Let the dipole be arbitrarily oriented, with components P_x, P_y, and P_z. We can then compute the magnetic field as the superposition of contributions from the 3 separate vector dipoles of moments $P_x\hat{i}$, $P_y\hat{j}$, and $P_z\hat{k}$, where $\hat{i}$, $\hat{j}$, and $\hat{k}$ denote unit vectors in the x, y and z directions.

According to Hertz' solution of Maxwell's equations, the electric and magnetic fields due to a radiating dipole may be expressed in terms of a dipole moment function (e.g., Sommerfeld, 1952; Abraham and Becker, 1937).

---

*The term "misdirection" appears in the text by Sommerfeld (1949).

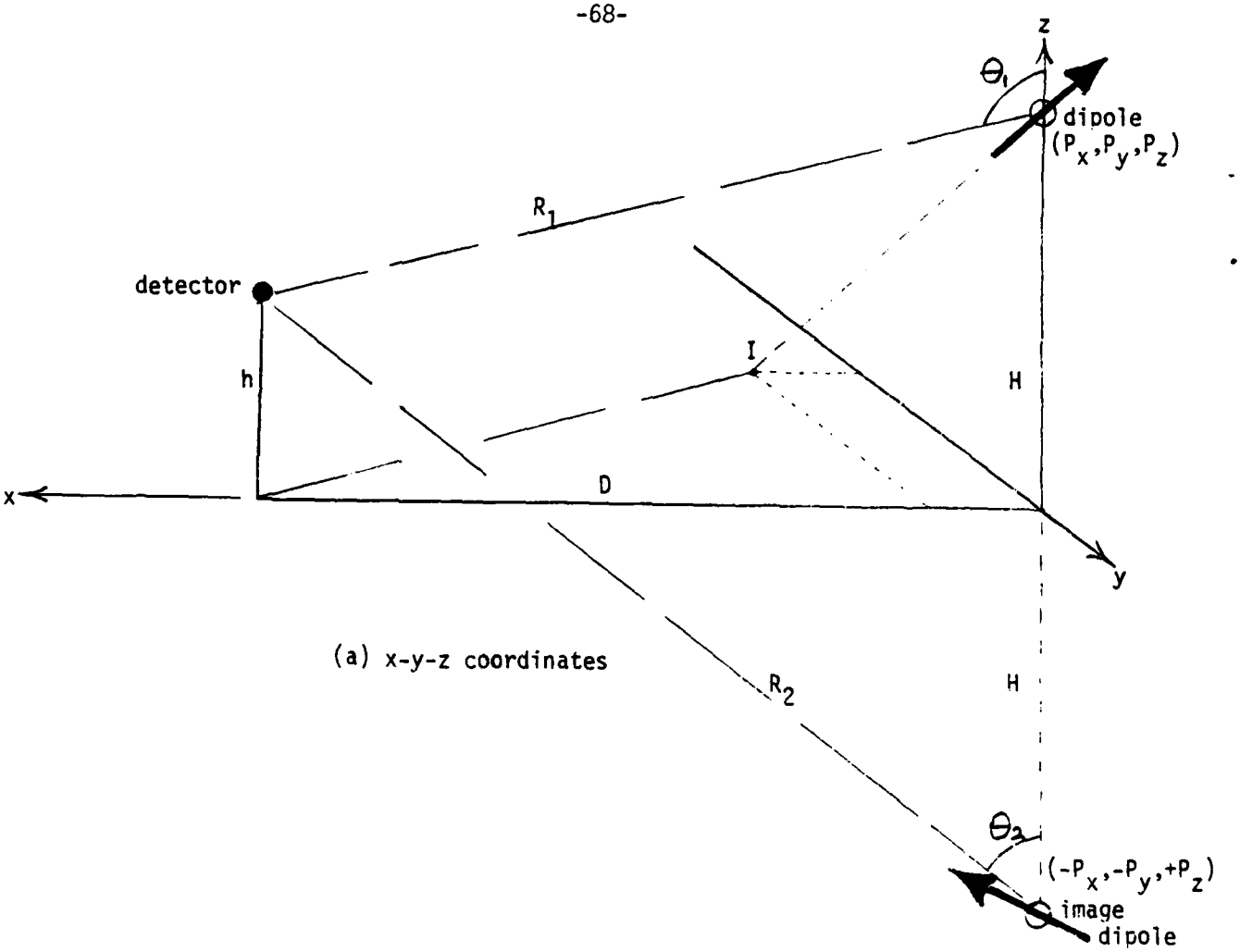

(a) x-y-z coordinates

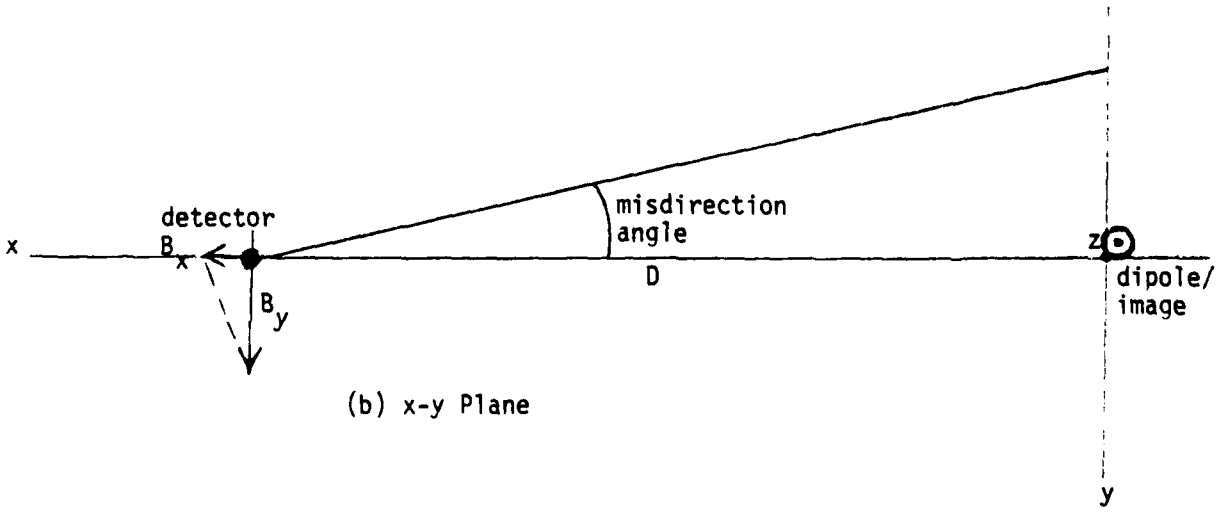

(b) x-y Plane

FIG. A-1. NONVERTICAL DIPOLE AND IMAGE

If we denote this time-dependent function by $\vec{P}(t-R/c)$, the vector potential $\vec{A}$ may be written as

$$\vec{A} = \frac{1}{R}\dot{\vec{P}}\,(t-R/c) \tag{1}$$

where the argument denotes the retarded time at distance R from the dipole, and the dot denotes differentiation with respect to the time. Here, the units adopted are Gaussian and $\dot{\vec{P}}$ is expressed in emu, i.e., abamp-cm, with R in cm. (In MKS units, an additional factor $\mu_o/4\pi$ appears on the right side, where μ_o is the magnetic permeability of free space, $4\pi x10^{-7}$ henry/meter; then $\dot{\vec{P}}$ is expressed in ampere-meters, with R in meters.)

Now the magnetic field intensity $\vec{B}$ is given by

$$\vec{B} = \text{curl}\ \vec{A}(R) = (\vec{R}/R) \times (d\vec{A}/dR) \tag{2}$$

since $\vec{A}$ is a function of R only. Differentiation yields

$$\frac{d\vec{A}}{dR} = -\frac{\dot{\vec{P}}}{R^2} - \frac{\ddot{\vec{P}}}{Rc} \tag{3}$$

where the second term results from the dependence of the time-like argument on R, and we obtain

$$\vec{B} = \vec{M}(R) \times \vec{R} \tag{4}$$

with

$$\vec{M}(R) \equiv \frac{1}{R}\left[\frac{\dot{\vec{P}}}{R^2} + \frac{\ddot{\vec{P}}}{Rc}\right] = \alpha\dot{\vec{P}} + \beta\ddot{\vec{P}} \tag{5}$$

so that $\alpha \equiv 1/R^3$ and $\beta \equiv 1/cR^2$.

In terms of our cartesian coordinates, let

$$\begin{aligned}
\vec{M}_1 &= M_{1x}\hat{i} + M_{1y}\hat{j} + M_{1z}\hat{k} \\
\vec{M}_2 &= M_{2x}\hat{i} + M_{2y}\hat{j} + M_{2z}\hat{k} \\
\vec{R}_1 &= D\hat{i} - (H-h)\hat{k} \\
\vec{R}_2 &= D\hat{i} + (H+h)\hat{k}
\end{aligned} \tag{6}$$

where $\hat{i}$, $\hat{j}$ and $\hat{k}$ denote unit vectors in the x, y and z directions; and $\vec{M}_1$ and $\vec{M}_2$ denote $\vec{M}_1(R_1)$ of the original dipole, and $\vec{M}_2(R_2)$ refers to its image, respectively. In this case, the components of $\dot{\vec{P}}_2$, $\ddot{\vec{P}}_2$ are related to those of $\dot{\vec{P}}_1$, $\ddot{\vec{P}}_1$ by:

$$\begin{aligned}
\dot{P}_{2x} &= -\dot{P}_{1x} \equiv -\dot{P}_x & \ddot{P}_{2x} &= -\ddot{P}_{1x} \equiv -\ddot{P}_x \\
\dot{P}_{2y} &= -\dot{P}_{1y} \equiv -\dot{P}_y & \ddot{P}_{2y} &= -\ddot{P}_{1y} \equiv -\ddot{P}_y \\
\dot{P}_{2z} &= +\dot{P}_{1z} \equiv +\dot{P}_z & \ddot{P}_{2z} &= +\ddot{P}_{1z} \equiv +\ddot{P}_z
\end{aligned} \tag{7}$$

where we identify the unsubscripted variables with the original dipole. It follows from (4) and (6) that, at the observer's position, the magnetic field of the original dipole is given by

$$\vec{B}_1 = [-(H-h)M_{1y}]\,\hat{i} + [(H-h)M_{1x} + D\,M_{1z}]\,\hat{j} + [-D\,M_{1y}]\,\hat{k} \tag{8}$$

while the magnetic field due to the image is given by

$$\vec{B}_2 = [(H+h)M_{2y}]\,\hat{i} + [-(H+h)M_{2x} + D\,M_{2z}]\,\hat{j} + [-D\,M_{2y}]\,\hat{k} \tag{9}$$

Hence, the sum of the two fields is:

$$\vec{B} = \vec{B}_1 + \vec{B}_2$$

$$= [(M_{2y} - M_{1y})H + (M_{2y} + M_{1y})h]\,\hat{i}$$

$$+ [-(M_{2x} - M_{1x})H - (M_{2x} + M_{1x})h + (M_{2z} + M_{1z})D]\,\hat{j}$$

$$+ [-(M_{2y} + M_{1y})D]\,\hat{k} \qquad (10)$$

For a vertical dipole, all components of $\vec{M}_1$ and $\vec{M}_2$ vanish except for M_{1z} and M_{2z}. Then $\vec{B}$ has only a y component, and there is no misdirection. When $\vec{B}$ has an x-component also, the misdirection angle is given by the arc tangent of $-B_x/B_y$ (Fig. A-1b). Consider the ratio $-B_x/B_y$, obtained from (10):

$$-\frac{B_x}{B_y} = \frac{-(M_{2y} - M_{1y})H - (M_{2y} + M_{1y})h}{-(M_{2x} - M_{1x})H - (M_{2x} + M_{1x})h + (M_{2z} + M_{1z})D} \qquad (11)$$

Using (5) and (7), we may rewrite (11) as:

$$-\frac{B_x}{B_y} = \frac{p_y H + q_y h}{p_x H + q_x h + p_z D} \qquad (12)$$

where

$$p_x = (\alpha_2 + \alpha_1)\dot{P}_x + (\beta_2 + \beta_1)\ddot{P}_x$$

$$p_y = (\alpha_2 + \alpha_1)\dot{P}_y + (\beta_2 + \beta_1)\ddot{P}_y$$

$$p_z = (\alpha_2 + \alpha_1)\dot{P}_z + (\beta_2 + \beta_1)\ddot{P}_z \qquad (13)$$

$$q_x = (\alpha_2 - \alpha_1)\dot{P}_x + (\beta_2 - \beta_1)\ddot{P}_x$$

$$q_y = (\alpha_2 - \alpha_1)\dot{P}_y + (\beta_2 - \beta_1)\ddot{P}_y$$

and where $\dot{P}_x$, $\ddot{P}_x$, $\dot{P}_y$, $\ddot{P}_y$, $\dot{P}_z$, $\ddot{P}_z$ refer to the original dipole components. Divide through numerator and denominator by $p_z D$, and note that we may write:

$$\dot{P}_x = \frac{P_x}{P}\dot{P}, \qquad \ddot{P}_x = \frac{P_x}{P}\ddot{P}$$

$$\dot{P}_y = \frac{P_y}{P}\dot{P}, \qquad \ddot{P}_y = \frac{P_y}{P}\ddot{P} \tag{14}$$

$$\dot{P}_z = \frac{P_z}{P}\dot{P}, \qquad \ddot{P}_z = \frac{P_z}{P}\ddot{P}$$

where P_x, P_y, P_z are the original dipole moment vector components, and where $\dot{P}$ and $\ddot{P}$ are the time-derivatives of the vector magnitude P. Then p_x/p_z, p_y/p_z, q_x/p_z, and q_y/p_z become, using (13) and (14):

$$\frac{p_x}{p_z} = \frac{P_x}{P_z}, \qquad \frac{p_y}{p_z} = \frac{P_y}{P_z}$$

$$\frac{q_x}{p_z} = Q\,\frac{P_x}{P_z}, \qquad \frac{q_y}{p_z} = Q\,\frac{P_y}{P_z} \tag{15}$$

where

$$Q \equiv \frac{(\alpha_2 - \alpha_1)\dot{P} + (\beta_2 - \beta_1)\ddot{P}}{(\alpha_2 + \alpha_1)\dot{P} + (\beta_2 + \beta_1)\ddot{P}}$$

$$= \frac{(1/R_2^3 - 1/R_1^3)\dot{P} + (1/R_2^2 - 1/R_1^2)\ddot{P}/c}{(1/R_2^3 + 1/R_1^3)\dot{P} + (1/R_2^2 + 1/R_1^2)\ddot{P}/c} \tag{16}$$

Finally, the ratio $-B_x/B_y$ may be written:

$$-\frac{B_x}{B_y} = \frac{G\,\frac{P_y}{P_z}}{1 + G\frac{P_x}{P_z}} \tag{17}$$

where

$$G \equiv \frac{H + Qh}{D} \tag{18}$$

If the detector is on the ground plane (h=0), the problem simplifies greatly, and we have $\alpha_1=\alpha_2$ and $\beta_1=\beta_2$, so that Q=0. Then G reduces simply to G=H/D, and we have

$$-\frac{B_x}{B_y} = \frac{\frac{H}{D}\frac{P_y}{P_z}}{1 + \frac{H}{D}\frac{P_x}{P_z}} \tag{19}$$

which is identical to the result given by Uman et al (1980 - see plots), re-expressed in our terms, for a detector on the ground plane. An equivalent result was also given earlier for this case by Kalakowsky and Lewis (1966).

If the ground plane is completely nonconducting (no image), then the case of the detector at altitude h above ground also simplifies greatly. In this case α_2 and β_2 vanish, and Q=-1. Then

$$-\frac{B_x}{B_y} = \frac{\frac{(H-h)}{D}\frac{P_y}{P_z}}{1 + \frac{(H-h)}{D}\frac{P_x}{P_z}} \tag{20}$$

That is, H is replaced in (19) by the "net altitude," H-h.

A geometric interpretation of (19) (or (20)) is obtained by rewriting (19) in the form

$$(D + H\frac{P_x}{P_z})\,B_x + H\frac{P_y}{P_z}B_y = 0 \tag{21}$$

This expression implies that the "misdirection," in the plane of the observer and perpendicular to $\vec{B}$ at the observer, passes through the point whose x,y,z coordinates are $-(P_x/P_z)H$, $-(P_y/P_z)H$, and zero. This point (indicated by the letter I in Fig. A-1a) is also the intercept of the extended line of the dipole with the z=0 plane. This simple geometric interpretation was pointed out by Kalakowsky and Lewis (1966).

In the case of harmonic radiation, of angular frequency ω, we may replace $\ddot{P}$ by $j\omega\dot{P}$ in (16), so that Q is given by the complex quantity, with $k \equiv \omega/c$:

$$Q = \frac{(1/R_2^3 - 1/R_1^3) + j(k/R_2^2 - k/R_1^2)}{(1/R_2^3 + 1/R_1^3) + j(k/R_2^2 + k/R_1^2)} \tag{22}$$

$$= - \frac{(x_1^3 - x_2^3) + jk(x_1^2 - x_2^2)}{(x_1^3 + x_2^3) + jk(x_1^2 + x_2^2)}$$

$$= - \frac{a + jb}{a' + jb'} \tag{23}$$

where $x = 1/R$ $\quad (x_1 = 1/R_1, \quad x_2 = 1/R_2)$

$$a = x_1^3 - x_2^3 \qquad b = k(x_1^2 - x_2^2)$$

$$a' = x_1^3 + x_2^3 \qquad b' = k(x_1^2 + x_2^2)$$

so that

$$Q = - \frac{(aa' + bb')}{(a')^2 + (b')^2} + \frac{j(ab' - ba')}{(a')^2 + (b')^2} \tag{24}$$

$$= \text{Re } Q + j \text{ Im } Q$$

APPENDIX B

Polarization Errors in Lightning Direction Finding by Magnetic Crossed loops: "Misdirection" Due to Wave Scattering by Nearby Metal Surfaces (Site Errors)

In this section we consider the bearing error in magnetic direction finding due to scattering of the incident electromagnetic wave by conducting surfaces near the detector. The incident magnetic vector is assumed here to be in the horizontal plane as produced by a vertical current source. (Appendix A treats the misdirection due to a nonvertical current source.) This incident magnetic field induces eddy currents in the nearby surfaces. These currents in turn produce a secondary magnetic field that results in a total magnetic vector of generally different (distorted) orientation. The crossed-loop detector is "misdirected" when it senses the distorted orientation and indicates an erroneous bearing. (The term "misdirection" is used in the text by Sommerfeld, 1949).

The following error analysis does not appear to have been published previously.

Evaluation of the scattering of incident electromagnetic waves is in general a difficult problem, even by perfectly conducting bodies of simple shape, e.g. spheres (Stratton, 1941). In principle, matrix equations of infinite order are to be solved for the expansion coefficients (expansion in vector spherical wave functions). The difficulties are greater for spheroids although the vector wave equation is separable and solutions are obtainable, in spheroidal coordinates (e.g., Taylor, 1967). In practice, of course, various limits are considered that reduce the problem to one of obtaining only a few coefficients of importance.

We employ here three approximations. The first consists of the replacement of the wave equation (complete set of Maxwell's equations) by the Laplace equation. This can be done if the wavelength is much larger than the dimension of the airplane, valid e.g. for frequencies below 500 kHz. (This magnetostatic approach was suggested by C. E. Baum.) The site error is computed by superimposing the surface fields due to orthogonal incident field components.

The second approximation consists of replacing the aircraft by a simple geometric form. The most flexible 3-dimensional geometric form that can be expressed by one coordinate of a 3-parameter coordinate system is

the 3-axial ellipsoid. Here solutions are expressed in elliptical integrals, that need special tables or computer programs for numerical evaluation. However, if we reduce the 3-axial ellipsoid to a 2-axial (rotationally symmetric) prolate spheroid or to an elliptical cylinder, simpler solutions expressed in terms of trigonometric functions (arc tangent) are obtained. In many cases these simplified mathematical models are sufficient to study conditions on the edges of the wings and on the tail fin (using the elliptical cylinder) and the condition on the fuselage and on the nose (using the prolate spheroid). Even if we reduce the elliptical cylinder to a circular cylinder the differences in the surface fields due to axial and transverse incident fields (the cause of the site error) is still significant, as will be shown. However, if we in turn reduce the prolate spheroid to a sphere these essential differences vanish because of the extreme symmetry of the sphere. Therefore, the sphere cannot be used to model the misdirection effect of an airplane body.

Our third approximation is the assumption that the aircraft is a good conductor, so that the magnetic field is excluded from the interior of the aircraft (by the induced skin currents). This is justifiable based on the fact that the skin depth (given by $6.6/\sqrt{\nu}$ cm in copper, where ν is the frequency (Stratton, 1941)) is only 0.03 cm at a frequency of 50 kHz, and is thus less than typical aircraft skin thicknesses (mm).

In the magnetostatic limit, the boundary condition at the aircraft surface is that the magnetic field be tangent to the surface (zero normal gradient). (Note that these are also the conditions in fluid "potential flow," so that the results of "potential flow" theory are applicable. See e.g. Hess, 1962.)

We adopt a cartesian coordinate system and show in Fig. B-1 an ellipsoid projected onto the x-y plane. It is aligned with the 3 axes, and has semi-axis lengths a, b, and c along the x, y and z axes, respectively. (The z axis is not shown.) We assume that the top of the airplane points in the +z direction, and that the incident magnetic field is parallel to the x-y plane. The incident wave propagates with angle of attack θ_0 with respect to the y-axis as shown, and with the magnetic field lines perpendicular to this direction. We will consider the magnetic field distortions at several points, such as A, B, C, and D in the figure. These can represent for example positions along the centerline on top of a fuselage or vertical tail fin, or along a wing.

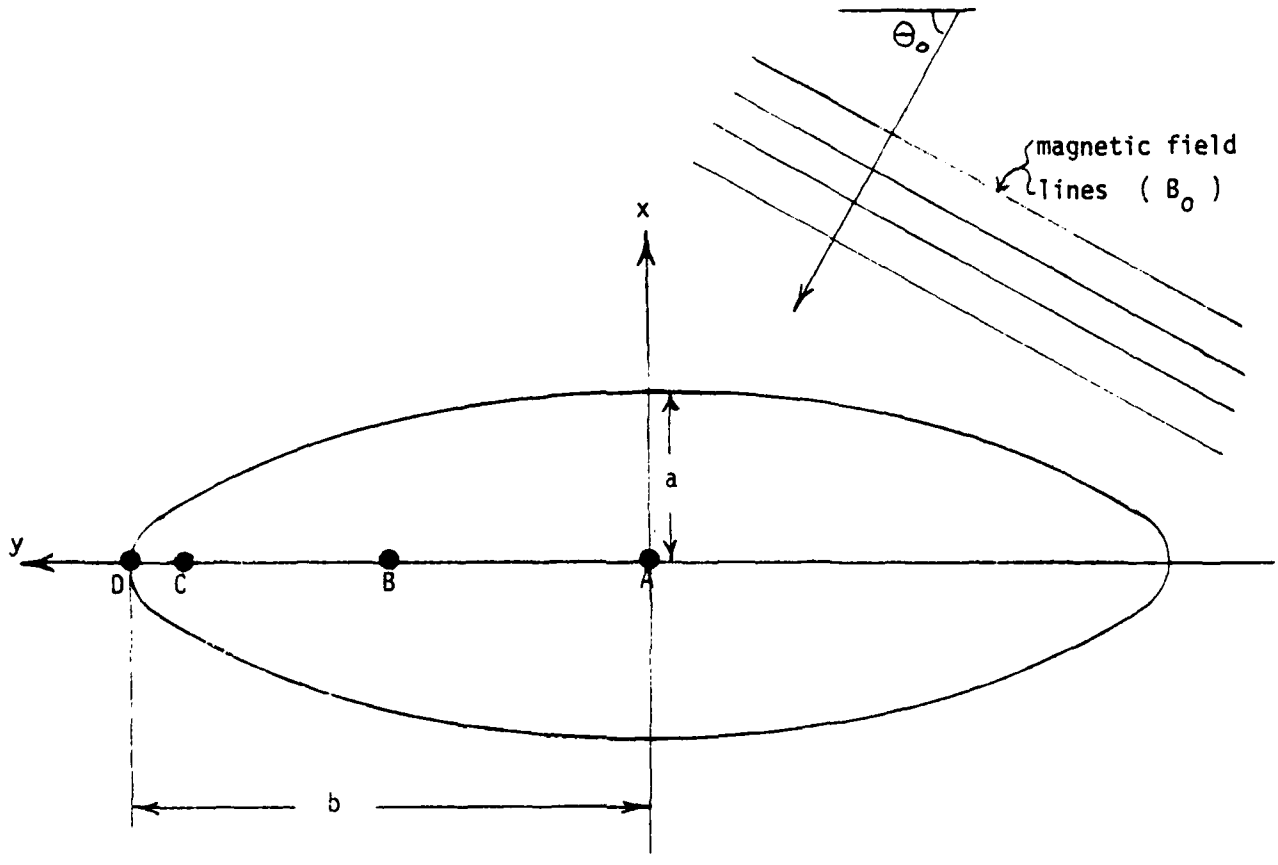

FIG. B-1. ELLIPSOID MODEL

● = detector positions along "top"

Later we will consider axially symmetric cases in which the y-axis is the axis of rotational symmetry. Thus we consider the solution to be a superposition of two primary solutions: One is the "transverse" case where $\theta_0=0^o$, the incident field being in the x-direction, perpendicular to the axis of symmetry. The other is the "axial" case where $\theta_0=90^o$, in which the incident field is in the y-direction, parallel to the axis of symmetry.

Before considering the general solutions for the spheroid or ellipsoid, let us first consider the limit in which b becomes infinite. The ellipsoid then elongates into a long cylinder or wire parallel to the y-axis and of constant elliptic cross-section, as shown in Fig. B-2.

A. CIRCULAR CYLINDER (c=a)

First we treat the circular cylinder, where c=a and b=∞, in the axial case where $\theta_0=90^o$. Here the field is parallel to the cylinder axis, and the solution becomes trivial. The field is excluded from the interior by a solenoidal sheet current in the surface, in the azimuthal direction about the axis. This current produces an internal field that cancels out the incident field, but the current produces no external field. Hence there is no distortion in the axial case, $\theta_0=90^o$.

Next we treat the circular cylinder transverse case, where $\theta_0=0$. Figure B-3a (App. B) shows the field ("flow") lines in this case. The solution of Laplace's equation that satisfies the boundary conditions at infinity and on the surface is the potential

$$\phi = - B_0 \cdot (r + a^2/r) \cdot \cos\psi \qquad (1)$$

where r denotes the cylindrical radial coordinate, a denotes the cylinder radius, B_0 denotes the magnetic field magnitude at infinity (large r), and ψ is the azimuthal angle about the cylinder axis ($\psi=0$ along the direction of $\vec{B}_0$). It may be readily verified that the potential (1) satisfies Laplace's equation,

$$\frac{\partial^2\phi}{\partial r^2} + \frac{1}{r}\frac{\partial\phi}{\partial r} + \frac{1}{r^2}\frac{\partial^2\phi}{\partial\psi^2} = 0 \qquad (2)$$

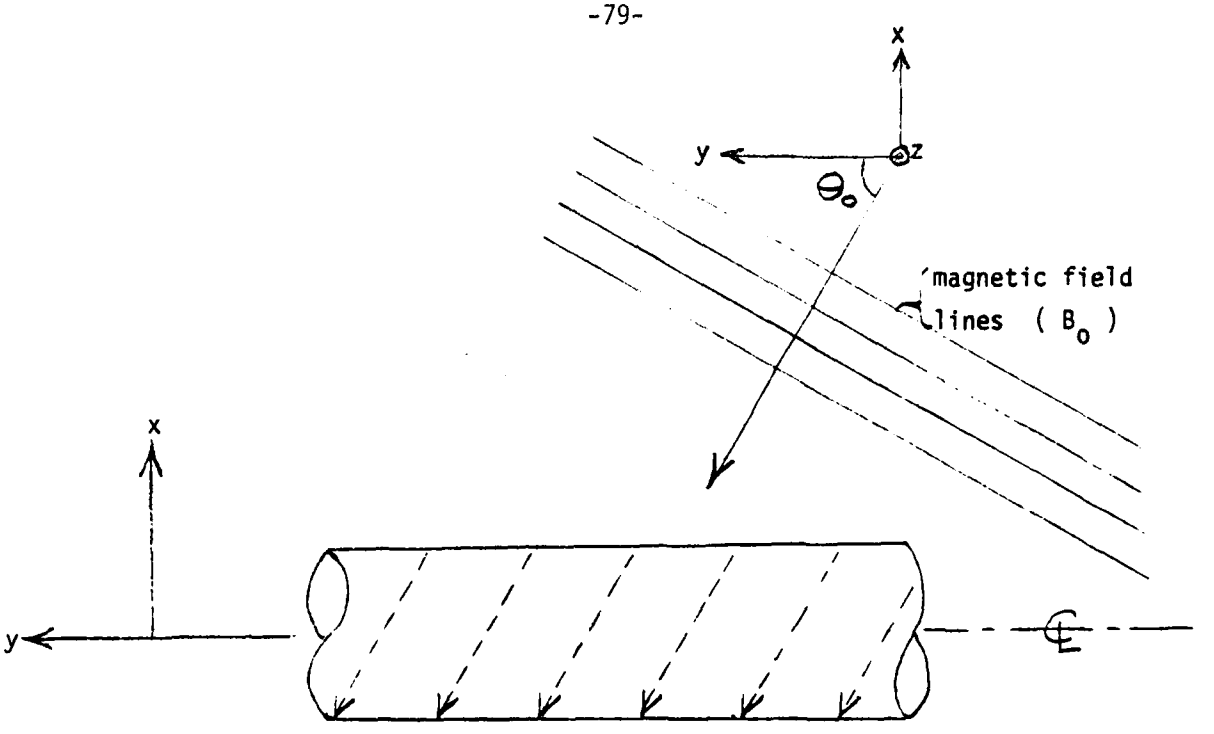

FIG. B-2. ELLIPTIC CYLINDER

----> = current flow planes

One boundary condition is that as r becomes large, ϕ approaches

$$\phi \sim - B_o\, r \cos\psi = - B_o x \tag{3}$$

representing the potential of the constant field $\vec{B}_o$ along the x-direction. On the surface the other boundary condition is that the normal component of the gradient vanishes, that is,

$$- \frac{\partial \phi}{\partial r} = + B_o\left(1 - \frac{a^2}{r^2}\right) \cos\psi \tag{4}$$

vanishes for all ψ when r=a. Thus (1) satisfies both boundary conditions.

The radial and azimuthal field components, B_r and B_ψ, are given by the components of the gradient,

$$B_r = - \frac{\partial \phi}{\partial r} = B_o \cdot \left(1 - \frac{a^2}{r^2}\right) \cdot \cos\psi \tag{5}$$

$$B_\psi = - \frac{1}{r} \frac{\partial \phi}{\partial \psi} = - B_o \left(1 + \frac{a^2}{r^2}\right) \cdot \sin\psi \tag{6}$$

The distorted field of interest is obtained by considering the x-component B_x at r=a, namely,

$$\begin{aligned} (B_x)_a &= B_r \cos\psi - B_\psi \sin\psi \\ &= B_o + B_o(2\sin^2\psi - 1)(a^2/r^2) \\ &= B_o + (2\sin^2\psi - 1)B_o \end{aligned} \tag{7}$$

where the first term on the right-hand side of (7) represents the undisturbed field, and the second term represents the distortion caused by the cylinder.

Thus, the perturbation field (addition to the incident field) goes from $+B_o$ on the "top" of the cylinder (where the dot in Fig. B-3 represents the probable position of the detector), to $-B_o$ on the "side" looking into the magnetic field. Assuming the crossed loop to be normally positioned (at the dot position) on "top", it senses a total field value $2B_o$, that is, enhanced by a factor 2.

Now we are in a position to calculate the misdirection at angle of attack θ_o. That is, or top of the cylinder B_x is enhanced by a factor 2, while B_y remains unaffected. Hence we have

$$\frac{B_y}{B_x} = \tan\theta = \frac{B_{oy}}{2B_{ox}} = \frac{1}{2}\tan\theta_o \tag{8}$$

as the definition of θ, and therefore

$$\theta - \theta_o = \arctan\ (\frac{1}{2}\ \tan\theta_o) - \theta_o \tag{9}$$

is the amount of misdirection or bearing error at angle of attack θ_o.

From (9) we note that the bearing error is zero (i.e., $\theta=\theta_o$) when $\theta_o=0$ and when $\theta_o=90^o$. The maximum error is -19.5^o (or $+19.5^o$) occurring when θ_o is 54.7^o (or its supplement 125.3^o). This follows from the vanishing of the derivative of (9) with respect to θ_o. The variation of bearing error with angle θ_o given by (9) is shown in Table 1.

At arbitrary angle of attack θ_o, the axial field component gives rise to skin currents flowing azimuthally around the cylinder, while the transverse field component gives rise to longitudinal currents, in the $\pm y$ directions on the two x-sides of the cylinder. Thus the resultant skin current flow-lines are ellipses whose planes are parallel to the z-axis and the direction of attack (i.e., skewed with respect to the cylinder axis, as shown in Fig. B-2).

B. ELLIPTIC CYLINDER ($c \neq a$)

In the more general elliptic cylinder case, the two principal fields are again in the x-direction ($\theta_o=0^o$, transverse), and the y-direction ($\theta_o=90^o$, axial). Again as in the circular cylinder, the axial field gives rise to no perturbation. In the transverse case, however, the field flow

is perturbed as shown in Fig. B-3, where in Figs. B-3b and B-3c, the flows are topologically similar to the circular case, Fig. B-3a. Figure B-3b (c<a) can represent a flat wing, with the detector (large dot in the middle) sensing relatively little field distortion. Figure B-3c (c>a) can represent a thin tail fin, where the detector (large dot on the edge) senses a large distortion.

It can be shown that for all cases in Fig. B-3 the misdirection is given by

$$\theta - \theta_o = \text{arc tan } (R \tan\theta_o) - \theta_o \tag{10}$$

where the "ratio-factor" R is defined by

$$R = \frac{a}{a+c} \tag{11}$$

Thus, R reduces to 1/2 when c=a as in Fig. B-3a, and (10) reduces to (9) for the circular cylinder. At the middle of a flat wing (Fig. B-3b) where c<<a, R reduces to approximately unity so that the distortion is minimal. On the edge of a thin tail fin (Fig. B-3c) where c>>a, R becomes small and θ becomes zero (due to the dominance of B_x which becomes large), independent of θ_o.

C. PROLATE SPHEROID

A prolate spheroid is a reasonable model for a fuselage of finite length. In this case (referring to Fig. B-1, where y is the axis of rotation), the radii are related by a=c, as in the circular cylinder, but b is now finite. Hence the results depend on the ratio t=a/b, which is less than unity for a prolate spheroid (but greater than unity for an oblate spheroid).

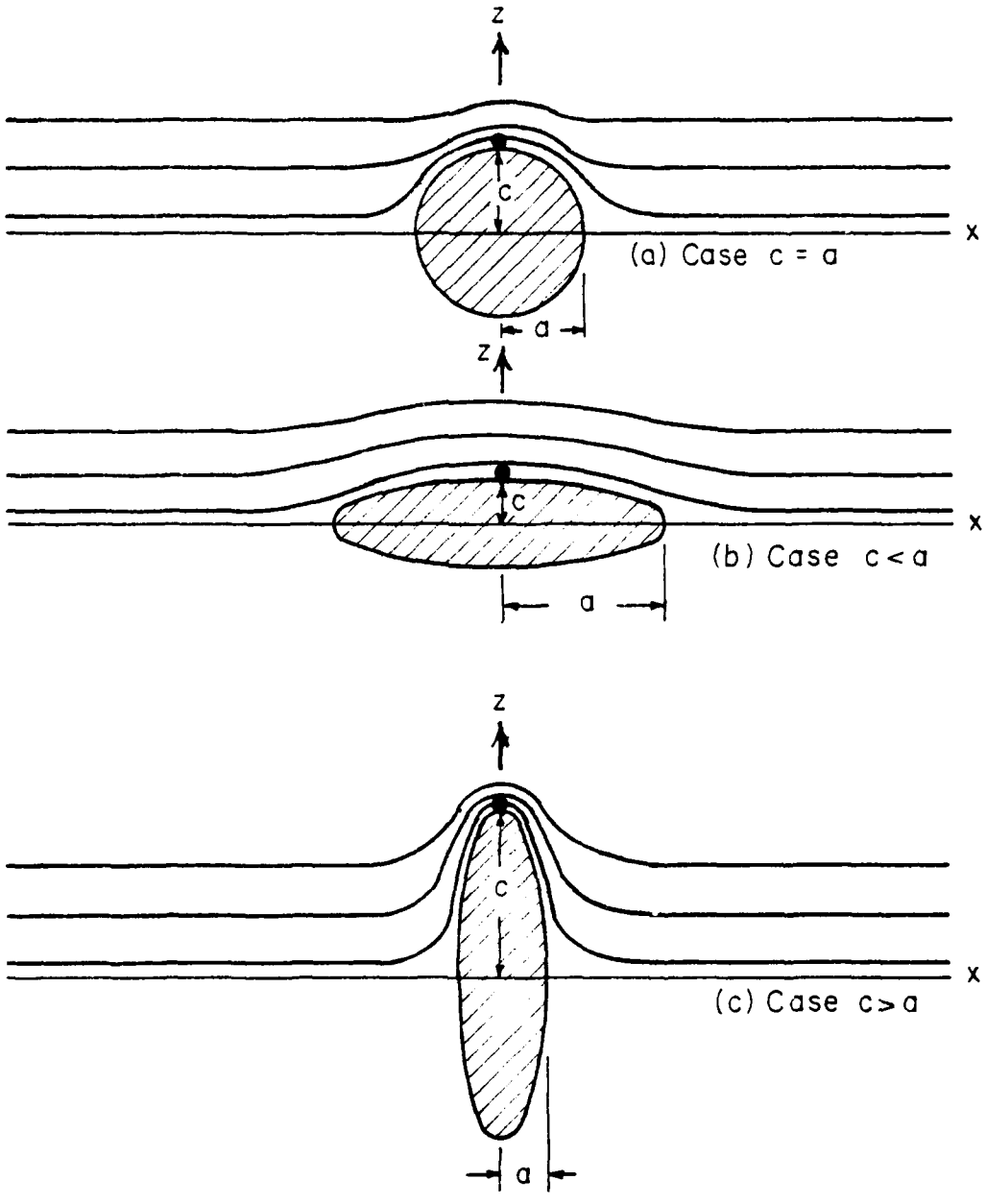

FIG. B-3. TRANSVERSE FIELD FLOW-LINES AROUND CYLINDER OF ELLIPTIC CROSS-SECTION ● = detector position on "top"

It can be shown that the ratio-factor R in (10) and (11) is now replaced by GR (see Eq. (15) below), where G is defined by

$$G(y,t) = (b^2 - y^2)^{1/2}/(b^2 - y^2 + t^2\, y^2)^{1/2} \tag{12}$$

where t=a/b, and y is the y-distance of the surface point from the mid-point; and R may be defined by

$$R(t) = 0.5\ (1 - 2t^2 + N)/(1 - N) \tag{13}$$

with N defined by

$$N = -\frac{t^2}{2\sqrt{1-t^2}}\ \ln\left[\frac{1 + \sqrt{1-t^2}}{1 - \sqrt{1-t^2}}\right] \tag{14}$$

Thus the misdirection is given by

$$\theta - \theta_o = \text{arc tan}\ (GR\ \tan\theta_o) - \theta_o \tag{15}$$

where G and R are given by (12) and (13). Note that G denotes the cosine of the tilt angle β of the tangent-plane with respect to the horizontal plane.

It is of interest to consider the limits t=1 and t=0. In the former (spherical) limit R becomes 1.0, and G becomes $(1-y^2/b^2)^{1/2}$ or $\cos\beta$, where β is the angle of tilt. In the latter limit R becomes 0.5, and G becomes unity, appropriate to the circular cylinder (GR=0.5, Eqs. (8) and (9)). The variation of R(t) with t, and the value of G at selected values of t and y/b, are shown in Table 2.

In Table 3 the variations of bearing error with angle θ_o are shown, with t and y/b as parameters. Here, y/b has the values 0, 0.5, 0.9, 0.99, and 1.0 (as in Table 2), corresponding to the positions labelled A, B, C, and D, respectively, in Fig. B-1 (positions along the top of the fuselage where positions y/b=0.99 and 1.0 are both denoted by the letter D).

D. T-39 MODEL SITE ERRORS

Numerical solutions using a computer model applied to realistic 3-dimensional aircraft geometries are presently underway. The model numerically solves the Laplace equation, in integral form, subject to the boundary conditions of uniform field at infinity and zero normal gradient at the aircraft surface. The aircraft surface is approximated by a multifaceted surface where each facet is a small quadrilateral panel, as illustrated in Figs. B-4 and B-5.

In the light of data obtained in 1977 by the Air Force Flight Dynamics Laboratory in flight tests of Stormscope (see p. 40) we employed our computer to obtain a preliminary assessment of the possible influence of site errors. The aircraft is a T-39, with the instrument installed near the leading edge of (and on the underside of) the right wing tip. The model portrayed in Figs. B-4 and B-5 shows the wing modeled reasonably realistically, while the fuselage, whose detailed structure should be unimportant in this case, is modeled crudely.

The panels in Figs. B-4 and B-5 are labelled by letters A-H, denoting various sections, with A and B on the fuselage, and C-G on the wing and H on the wingtip. Each section has 12 panels, with Nos. 1-6 on the upper surface and Nos. 7-12 denoting image positions on the under surface (with 7 under 6, 8 under 5, ..., and 12 under 1). The Stormscope instrument position is on Panel G-11.

Some selected preliminary results are as follows, indicating panel location, maximum misdirection, and angle of incidence at which this occurs. For each section we give the optimum location.

A - 9: $+11^{\circ}$ at 135° (bottom of fuselage at midwing)

B: (no good location, vertical plane)

C - 3: $+16^{\circ}$ at 30° (top of wing, behind leading edge)
C - 10: $+18^{\circ}$ at 5° (bottom of wing, behind leading edge)

D - 2: $+8^{\circ}$ at 15° (top of wing, adjacent to leading edge)
D - 11: $+12^{\circ}$ at 5° (bottom of wing, adjacent to leading edge)

E - 11: $+5^{\circ}$ at 15° (bottom of wing, adjacent to leading edge)
E - 2: $+10^{\circ}$ at 160° (top of wing, adjacent to leading edge)

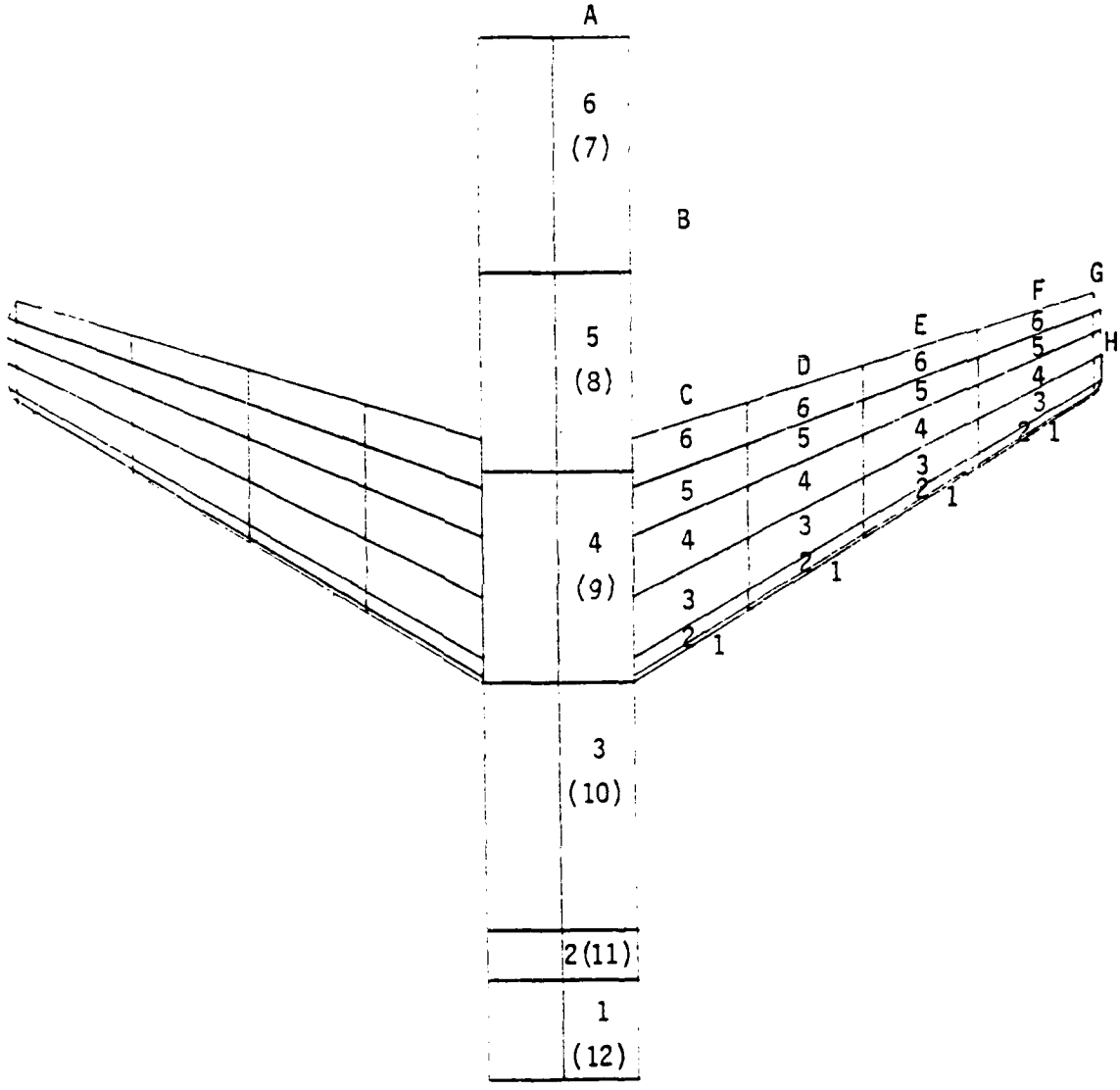

FIG. B-4. T-39 COMPUTER MODEL. PLAN VIEW.

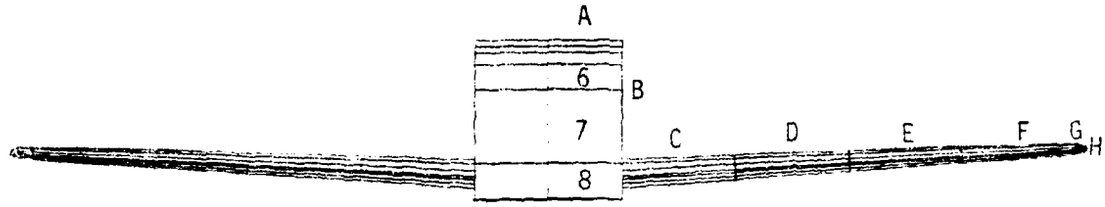

REAR VIEW

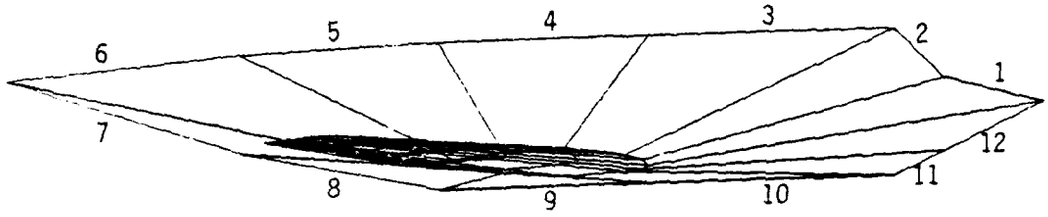

SIDE VIEW

SIDE OF FUSELAGE (SECTION B)

(showing underside as well as topside)

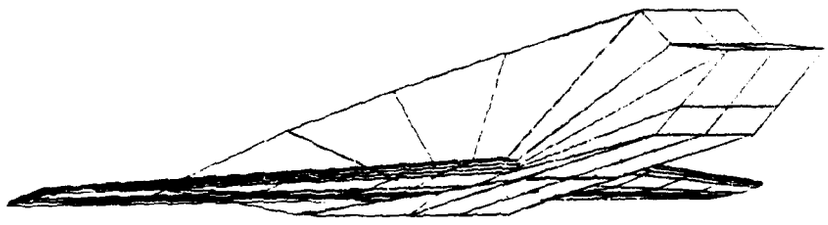

FIG. B-5. T-39 COMPUTER MODEL. OTHER VIEWS.

F - 5: $+3^{o}$ at 110^{o} (top of wing, ahead of trailing edge)
F - 10: $+3^{o}$ at 25^{o} (bottom of wing, behind leading edge)

G - 10: $+4^{o}$ at 80^{o} (adjacent to wingtip, bottom, behind leading edge)
G - 3: $+6^{o}$ at 115^{o} (adjacent to wingtip, top, behind leading edge)

G - 11: -7^{o} at 170^{o} (Stormscope location, bottom, leading corner of wingtip)
G - 2: $+10^{o}$ at 95^{o} (mirror of Stormscope location, top surface)

H: (no good location, vertical plane)

The foregoing represent optimum locations (where the misdirections are minimal). The misdirections are larger at other locations.

The following conclusions may be drawn. The optimum fuselage location is underneath, at midwing position. The optimum locations on the wing (and in fact on the whole airplane) are near the wingtip and away from the fuselage, either on top and ahead of the trailing edge, or underneath and behind the leading edge. The actual Stormscope location used was a not unreasonable choice (in the absence of data on site errors) but could have been improved. The reported bearing discrepancies (Baum and Seymour, 1980) are consistent with the computed maximum misdirection near the wingtip, of the order of 10^{o}.

It should be mentioned that these figures apply to an incident field lying entirely in the horizontal plane. The presence of a vertical field component would be associated with a slanted lightning channel. In this way the error due to slant would be coupled with site error. It is straightforward to include the vertical component in the calculations, i.e. to study the site errors associated with slanted channels, in a subsequent extension of the present work.

The overall agreement between the analytical calculations (e.g. using cylinder and ellipsoid models) and the numbers obtained from the computer model is satisfying. However, it is evident that more detailed information can be obtained with the computer model calculations. The analytical calculations are limited to simple analytical shapes, whereas with the computer model one can treat more realistic airplane shapes.

AD-A095 354 PARKER (LEE W) INC CONCORD MASS F/G 1/2
AIRBORNE LIGHTNING WARNING SYSTEMS: A SURVEY.(U)
JUL 80 L W PARKER, H W KASEMIR F19628-79-C-0161
UNCLASSIFIED AFGL-TR-80-0226 NL

2 OF 2
AD A095 354

END
DATE FILMED
3 81
DTIC

Table 1. MISDIRECTION ON CIRCULAR CYLINDER

θ_o (degrees)	$\Delta\theta$ = misdirection (Eq. (9)) (degrees)
0	0.
5	- 2.50
10	- 4.96
15	- 7.37
20	- 9.69
25	-11.88
30	-13.90
35	-15.70
40	-17.24
45	-18.43
50	-19.21
55	-19.47
60	-19.11
65	-18.00
70	-16.05
75	-13.19
80	- 9.43
85	- 4.92
90	0.

Table 2. MISDIRECTION CONSTANT R VS t, AND
POSITION FACTOR G VS t AND y/b,
ON PROLATE SPHEROID

t=a/b	R(t)	Point A* G(y=0)	Point B* G(y=0.5b)	Point C* G(y=0.9b)	——— G(y=0.99b)	Point D* G(y=b)
0.	0.5	1.0	1.0	1.0	1.0	-
0.1	0.5207	1.0	0.998	0.979	0.819	0.
0.2	0.5591	1.0	0.993	0.924	0.580	0.
0.3	0.6054					
0.4	0.6563					
0.5	0.7100	1.0	0.961	0.696	0.274	0.
0.6	0.7658					
0.7	0.8230					
0.8	0.8812					
0.9	0.9403					
1.0	1.0	1.0†	0.866†	0.436†	0.141†	0.†

*Positions A, B, C and D shown in Fig. B-1 (y=0.99b not shown).

†cos (arc sin y/b) for sphere.

Table 3a. MISDIRECTION AT POSITIONS ON PROLATE SPHEROID
(FIG. B-1, t=a/b=0.1)

θ_o (degrees)	$\Delta\theta$(y=0) GR=0.521	$\Delta\theta$(y=0.5b) GR=0.520	$\Delta\theta$(y=0.9b) GR=0.510	$\Delta\theta$(y=0.99b) GR=0.426	$\Delta\theta$(y=b) GR=0.
0	0.	0.	0.	0.	0.
5	- 2.39	- 2.40	- 2.45	- 2.87	- 5.0
10	- 4.75	- 4.76	- 4.86	- 5.70	-10.0
15	- 7.05	- 7.07	- 7.22	- 8.49	-15.0
20	- 9.26	- 9.28	- 9.48	-11.19	-20.0
25	-11.34	-11.37	-11.62	-13.76	-25.0
30	-13.26	-13.29	-13.59	-16.18	-30.0
35	-14.96	-14.99	-15.35	-18.39	-35.0
40	-16.39	-16.43	-16.83	-20.33	-40.0
45	-17.48	-17.53	-17.98	-21.93	-45.0
50	-18.16	-18.21	-18.71	-23.08	-50.0
55	-18.35	-18.40	-18.93	-23.68	-55.0
60	-17.94	-17.99	-18.54	-23.58	-60.0
65	-16.83	-16.88	-17.44	-22.59	-65.0
70	-14.94	-14.99	-15.51	-20.51	-70.0
75	-12.22	-12.26	-12.72	-17.17	-75.0
80	- 8.70	- 8.73	- 9.07	-12.49	-80.0
85	- 4.53	- 4.55	- 4.73	- 6.61	-85.0
90	0.	0.	0.	0.	-

Table 3b. MISDIRECTION AT POSITIONS ON PROLATE SPHEROID
(FIG. B-1, t=a/b=0.2)

θ_o (degrees)	$\Delta\theta$(y=0) GR=0.559	$\Delta\theta$(y=0.5b) GR=0.555	$\Delta\theta$(y=0.9b) GR=0.517	$\Delta\theta$(y=0.99b) GR=0.324	$\Delta\theta$(y=b) GR=0.
0	0.	0.	0.	0.	0.
5	- 2.20	- 2.22	- 2.41	- 3.38	- 5.0
10	- 4.37	- 4.41	- 4.79	- 6.73	-10.0
15	- 6.48	- 6.54	- 7.11	-10.04	-15.0
20	- 8.50	- 8.58	- 9.34	-13.27	-20.0
25	-10.39	-10.49	-11.45	-16.41	-25.0
30	-12.11	-12.23	-13.38	-19.40	-30.0
35	-13.62	-13.76	-15.10	-22.22	-35.0
40	-14.87	-15.03	-16.55	-24.79	-40.0
45	-15.79	-15.97	-17.66	-27.05	-45.0
50	-16.33	-16.52	-18.36	-28.89	-50.0
55	-16.40	-16.60	-18.56	-30.17	-55.0
60	-15.93	-16.13	-18.16	-30.70	-60.0
65	-14.83	-15.04	-17.05	-30.21	-65.0
70	-13.07	-13.26	-15.15	-28.33	-70.0
75	-10.61	-10.77	-12.40	-24.59	-75.0
80	- 7.51	- 7.63	- 8.83	-18.56	-80.0
85	- 3.90	- 3.96	- 4.60	-10.11	-85.0
90	0.	0.	0.	0.	-

Table 3c. MISDIRECTION AT POSITIONS ON PROLATE SPHEROID
(FIG. B-1, t=a/b=0.5)

θ_o (degrees)	$\Delta\theta$(y=0) GR=0.710	$\Delta\theta$(y=0.5b) GR=0.682	$\Delta\theta$(y=0.9b) GR=0.494	$\Delta\theta$(y=0.99b) GR=0.1945	$\Delta\theta$(y=b) GR=0.
0	0.	0.	0.	0.	0.
5	- 1.45	- 1.59	- 2.53	- 4.03	- 5.0
10	- 2.86	- 3.14	- 5.02	- 8.04	-10.0
15	- 4.23	- 4.64	- 7.46	-12.02	-15.0
20	- 5.51	- 6.06	- 9.81	-15.95	-20.0
25	- 6.68	- 7.36	-12.03	-19.82	-25.0
30	- 7.71	- 8.51	-14.08	-23.59	-30.0
35	- 8.57	- 9.47	-15.92	-27.24	-35.0
40	- 9.22	-10.22	-17.49	-30.73	-40.0
45	- 9.63	-10.71	-18.71	-33.99	-45.0
50	- 9.76	-10.90	-19.51	-36.95	-50.0
55	- 9.60	-10.75	-19.80	-39.48	-55.0
60	- 9.12	-10.25	-19.45	-41.38	-60.0
65	- 8.30	- 9.36	-18.35	-42.36	-65.0
70	- 7.14	- 8.09	-16.38	-41.88	-70.0
75	- 5.68	- 6.45	-13.48	-39.02	-75.0
80	- 3.95	- 4.50	- 9.64	-32.19	-80.0
85	- 2.02	- 2.31	- 5.04	-19.22	-85.0
90	0.	0.	0.	0.	-

Table 3d. MISDIRECTION AT POSITIONS ON PROLATE SPHEROID
(FIG. B-1, t=a/b=1.0 for sphere)

θ_U (degrees)	$\Delta\theta$(y=0) GR=1.0	$\Delta\theta$(y=0.5b) GR=0.866	$\Delta\theta$(y=0.9b) GR=0.436	$\Delta\theta$(y=0.99b) GR=0.141	$\Delta\theta$(y=b) GR=0
0	0.	0.	0.	0.	0.
5	0.	- 0.67	- 2.82	- 4.29	- 5.0
10	0.	- 1.32	- 5.60	- 8.58	-10.0
15	0.	- 1.94	- 8.34	-12.84	-15.0
20	0.	- 2.50	-10.99	-17.06	-20.0
25	0.	- 3.01	-13.51	-21.24	-25.0
30	0.	- 3.43	-15.87	-25.34	-30.0
35	0.	- 3.77	-18.03	-29.36	-35.0
40	0.	- 3.99	-19.91	-33.25	-40.0
45	0.	- 4.11	-21.45	-36.97	-45.0
50	0.	- 4.10	-22.55	-40.46	-50.0
55	0.	- 3.96	-23.10	-43.61	-55.0
60	0.	- 3.69	-22.95	-46.27	-60.0
65	0.	- 3.30	-21.93	-48.17	-65.0
70	0.	- 2.80	-19.86	-48.81	-70.0
75	0.	- 2.19	-16.58	-47.23	-75.0
80	0.	- 1.51	-12.02	-41.34	-80.0
85	0.	- 0.77	- 6.35	-26.81	-85.0
90	0.	0.	0.	0.	-

REFERENCES

1. Abraham, M. and R. Becker, The Classical Theory of Electricity and Magnetism, Blackie & Son, Ltd., London (1937).

2. Battan, L. J., Radar Observation of the Atmosphere, Univ. of Chicago Press, Chicago (1973).

3. Baum, C. E., On the singularity expansion method for the solution of electromagnetic interaction problems, Interaction Note 88, AFWL (1971).

4. Baum, R. K. and T. J. Seymour, In-flight evaluation of a severe weather avoidance system for aircraft, AFFDL Report AFWAL-TR-80-3022, May (1980).

5. Bent, R. B., A new approach to lightning positioning and tracking, FAA/FIT Workshop on Grounding and Lightning Technology, Melbourne, Florida, Report FAA-RD-79-6 supplement 1A (1979).

6. Chalmers, J. A., Atmospheric Electricity, Pergamon Press, New York (1967).

7. Chapman, S., Corona-point discharge in wind and application to thunderclouds, Recent Advances in Atmospheric Electricity, L. G. Smith, Ed., Pergamon Press (1959). pp. 277-288. See also Chapman, S., The magnitude of corona-point discharge current, J. Atmos. Sci. 34, 1801-1809 (1977).

8. Clark, J. F., Airborne measurement of atmospheric potential gradient, J. Geophys. Res. 62, 617-628 (1957).

9. Clifford, D. W., Aircraft mishap experience from atmospheric electricity hazards, Agard Lecture Series No. 110, Atmospheric Electricity - Aircraft Interaction (1980).

10. Cobb, W. E. and F. J. Holitza, A note on lightning strikes to aircraft, Mon. Wea. Rev. 96, 807-808 (1968).

11. Corn, P. B., Lightning as a hazard to aviation, Amer. Meteor. Soc. 11th Conf. on Severe Local Storms, Kansas City, MO, Oct. 2-5 (1979).

11a. DuBro, G. A., Editor, Agard Lecture Series No. 110, Atmospheric Electricity - Aircraft Interaction (1980).

12. Edgar, B. C., State of technology in optical systems, in Proceedings: Workshop on the Need for Lightning Observations from Space, NASA Report NASA CP-2095, L. S. Christensen, W. Frost and W. W. Vaughan, Eds., July (1979). pp. 81-87. See also Turman, B. N., A review of satellite lightning experiments, same report, pp. 61-80.

13. Fisher, F. A. and J. A. Plumer, Lightning protection of aircraft, NASA Reference Publication 1008 October (1977).

14. Fitzgerald, D. R., Measurement techniques in clouds, in Problems of Atmospheric and Space Electricity, S. C. Coroniti, Ed., Elsevier, Amsterdam (1965). pp. 199-214.

15. Fitzgerald, D. R., Probable aircraft "triggering" of lightning in certain thunderstorms, Mon. Wea. Rev. 95, 835-842 (1967).

16. Fitzgerald, D. R., USAF flight lightning research, Proceedings, Lightning and Static Electricity Conference, 1968. AFAL Report AFAL-TR-68-290 Part II (1969).

17. Fitzgerald, D. R., Aircraft and rocket triggered natural lightning discharges, 1970 Lightning and Static Electricity Conference, AFAL Report (1970).

18. Fitzgerald, D. R., Some relationships of lightning to radar echoes, in Hq. AWS Aerospace Sciences Review, Report AWSRP 105-2, 78-4, Dec. (1978).

19. Golde, R. H., Lightning currents and related parameters, in Lightning, Vol. 1, R. H. Golde, Ed., Academic Press, New York (1977). pp. 309-350.

20. Griffiths, R. F. and B. Vonnegut, Tape recorder photocell instrument for detecting and recording lightning strokes, Weather, 254-257, Aug. (1975).

21. Gunn, R., (Basic Field Mill patent, first installed in dirigible U.S.S. Los Angeles, 1930), U.S. Patent No. 1,919,215, June 25 (1933).

22. Harrison, H. T., UAL Turbojet experience with electrical discharges, UAL Meteorological Circular No. 57, United Airlines, Chicago, Ill., January (1965).

23. Harvey, R. B. and E. A. Lewis, Radio mapping of 250 to 925 MHz noise sources in clouds, AFCRL Report AFCRL-72-0078, Jan. (1972).

24. Hayenga, C. O., Positions and movement of VHF lightning sources determined with microsecond resolution by interferometry, Ph.D. Thesis, Univ. of Colorado, Dept. of Astro-Geophysics (1979).

25. Hess, J. L., Calculation of potential flow about bodies of revolution having axes perpendicular to the free-stream direction, J. Aerospace Sci. 29, 726-742 (1962).

26. Holitza, F. J. and H. W. Kasemir, Accelerated decay of thunderstorm electric fields by chaff seeding, J. Geophys. Res. 79, 425-429 (1974).

27. Horner, F., The accuracy of the location of sources of atmospherics by radio direction-finding, Proc. Instn. Elec. Engrs., Pt. III, 101, 383-390 (1954).

28. Horner, F., Very-low-frequency propagation and direction-finding, Proc. Instn. Elec. Engrs. 104, Part B, 73-80 (1957).

29. Horner, F., The design and use of instruments for counting local lightning flashes, Proc. Instn. Elec. Engrs. 107, Part B, 321-330 (1960).

30. Horner, F., Radio noise from thunderstorms in Advances in Radio Research, Vol. 2, J. A. Saxton, Ed., Academic Press, New York (1964). pp. 121-204.

31. Israël, H., Atmospheric Electricity, (transl. from German, Israel Program for Scientific Translations), National Technical Information Service. No. TT-67-51394/1, Vol. 1 (1971), and TT-67-51394/2, Vol. 2 (1973).

32. Johnson, R. L., D. E. Janota and J. E. Hay, A study of the comparative performance of six lightning warning systems, in Lightning Technology, NASA Conference Publication 2128, FAA-RD-80-30 (1980). pp. 187-203.

33. Kalakowsky, C. B. and E. A. Lewis, VLF sferics of very large virtual source strength, AFCRL-66-629 (1966).

34. Kasemir, H. W., cited in footnote by Lueder, H., Electric recording of approaching thunderstorms and the fine structures of the atmospheric electric thunderstorm field (transl. from German), Meteor. Z. 60, 340-351 (1943).

35. Kasemir, H. W., Analysis of the electrostatic field of a lightning stroke, U.S. Army Electronics R and D Laboratory Technical Report 2321, Nov. (1962).

36. Kasemir, H. W., The cylindrical field mill, Meteorologische Rundschau 25, 33-38 (1972). (Cites earlier work by Matthias (1926) and Kasemir (1944 and 1951)).

37. Kasemir, H. W., Electric field measurements from airplanes, American Meteorological Society Fourth Symposium on Meteorological Observations and Instrumentation, Denver, Colorado, Apr. 10-14 (1978).

38. Kasemir, H. W., F. J. Holitza, W. E. Cobb and W. D. Rust, Lightning suppression by chaff seeding at the base of thunderstorms, J. Geophys. Res. 81, 1965-1970 (1976).

39. Kasemir, H. W. and F. Perkins, Lightning trigger field of the Orbiter, KSC Contract CC 69694A Final Report, NOAA, Oct. (1978).

40. Kidder, R. E., The location of lightning flashes at ranges less than 100 km, J. Atmos. Terr. Phys. 35, 283-290 (1973).

41. Kohl, D. A., Direction Finder, U.S. Patent No. 3,242,495, March 22 (1966).

42. Kohl, D. A., A 500-kHz sferics range detector, J. Appl. Meteor. 8, 610-617 (1969).

43. Krider, E. P., R. C. Noggle and M. A. Uman, A gated wideband magnetic direction-finder for lightning return strokes, J. Appl. Meteor. 15, 302-306 (1976). See also Krider, E. P., R. C. Noggle, A. E. Pifer and D. L. Vance, Lightning direction-finding systems for forest fire detection, Bull. Amer. Meteor. Soc. 61, 980-986 (1980).

44. Lee, K. S. H., Editor, EMP Interaction: Principles, techniques and reference data (EMP Interaction 2-1), AFWL TR-79-403 (1979).

45. Lewis, E. A., R. B. Harvey and J. E. Rasmussen, Hyperbolic direction finding with sferics of transatlantic origin, AFCRL Report AFCRL-62-178 (1962).

45a. Loeb, L. B., Electrical Coronas, U. Calif. Press, Berkeley (1965).

46. Markson, R., Ionospheric potential variations obtained from aircraft measurements of potential gradient, J. Geophys. Res. 81, 1980-1990 (1976).

47. Mason, B. J., The Physics of Clouds, Clarendon Press, Oxford (1971).

48. Maxwell, K. J., L. C. Walko and V. L. Mangold, In-flight measurements of lightning characteristics, FAA/FIT Workshop on Grounding and Lightning Technology, Melbourne, Florida, Report FAA-RD-79-6 (1979). pp. 113-120.

49. Musil, D. J. and J. Prodan, Direct effects of lightning on an aircraft during intentional penetrations of thunderstorms, in Lightning Technology, NASA Conference Publication 2128, FAA-RD-80-30 (1980). pp. 363-370.

50. Nanevicz, J. E., R. T. Bly, Jr. and R. C. Adamo, Airborne measurement of electromagnetic environment near thunderstorm cells (TRIP-1976), Technical Report AFFDL-TR-77-62, Aug. (1977).

51. Newman, M. M. and J. D. Robb, Protection for aircraft, in Lightning, Vol. 2, R. H. Golde, Ed., Academic Press, New York (1977). pp. 659-696.

52. Pierce, E. T., Electrostatic field changes due to lightning, Quart. J. Roy. Meteor. Soc. 81, 211-228 (1955).

53. Pierce, E. T., Some techniques for locating thunderstorms from a single observing station, in Vistas in Astronomy, A. Beer, Ed., Vol. 2, Pergamon Press, Oxford (1956). pp. 850-855.

54. Pierce, E. T., Atmospherics and radio noise, in Lightning, Vol. 1, R. H. Golde, Ed., Academic Press, New York (1977a). pp. 351-384.

55. Pierce, E. T., Lightning warning and avoidance, in Lightning, Vol. 2, R. H. Golde, Ed., Academic Press, New York (1977b). pp. 497-519.

56. Pitts, F. L., R. M. Thomas, K. P. Zaepfel, M. E. Thomas and R. E. Campbell, In-flight lightning characteristics measurement system, FAA/FIT Workshop on Grounding and Lightning Technology, Melbourne, Florida, Report FAA-RD-79-6 (1979). pp. 105-111.

57. Poehler, H. A., A preliminary test of the application of the lightning detection and ranging system (LDAR) as a thunderstorm warning and location device for the FAA including a correlation with updrafts, turbulence, and radar precipitation echoes, RCA Service Company, NASA Contractor Report CR-154629 for NASA Kennedy Space Center (1978).

57a. Poehler, H. A. and C. L. Lennon, Lightning detection and ranging system LDAR/System description and performance objectives, NASA Tech. Memo 74105, 20 June (1979).

58. Rozelle, R., Weather avoidance, an alternative to radar, The AOPA Pilot, Nov. (1979). pp. 95-105.

59. Ruhnke, L. H., Distance to lightning strokes as determined from electrostatic field strength measurements, J. Appl. Meteor. 1, 544-547 (1962).

60. Ruhnke, L. H., Determining distance to lightning strokes from a single station, NOAA Technical Report ERL 195-APCL 16, Jan. (1971a).

61. Ruhnke, L. H., A rocket-borne instrument to measure electric fields inside electrified clouds, NOAA Technical Report ERL 206-APCL 20, May (1971b).

62. Ryan, P. A. and N. Spitzer, Stormscope, U.S. Patent No. 4,023,408, May 17 (1977).

63. Schäfer, J., H. Volland, P. Ingmann, A. J. Eriksson and G. Heydt, A network of automatic atmospherics analysators, in Lightning Technology, NASA Conference Publication 2128, FAA-RD-80-30 (1980). pp. 215-225.

64. Seymour, T. J. and R. K. Baum, Evaluation of the Ryan Stormscope as a severe weather avoidance system for aircraft - preliminary report, FAA/FIT Workshop on Grounding and Lightning Technology, Melbourne, Florida, Report FAA-RD-79-6 (1979). pp. 29-35.

65. Simpson, G. C. and F. J. Scrase, The distribution of electricity in thunderclouds, Proc. Roy. Soc. London A161, 309-352 (1937).

66. Simpson, G. C. and G. D. Robinson, The distribution of electricity in thunderclouds II, Proc. Roy. Soc. London A177, 281-329 (1941).

67. Smith, L. G., Electric field meter with extended frequency range, Rev. Sci. Instrum. 25, 510-513 (1954).

68. Sommerfeld, A., Partial Differential Equations in Physics, Lectures on Theoretical Physics, Vol. 6, Academic Press, New York (1949).

69. Sommerfeld, A., Electrodynamics, Lectures on Theoretical Physics, Vol. 3, Academic Press, New York (1952).

70. Stergis, C. G. and J. W. Doyle, Location of near lightning discharges, in Recent Advances in Atmospheric Electricity, L. G. Smith, Ed., Pergamon Press (1959). pp. 589-597.

71. Stratton, J. A., Electromagnetic Theory, McGraw-Hill, New York (1941).

72. Taylor, C. D., On the exact theory of a prolate spheroid receiving and scattering antenna, Radio Sci. 2, 351-360 (1967).

73. Taylor, W. L., A VHF technique for space-time mapping of lightning discharge processes, J. Geophys. Res. 83, 3575-3583 (1978).

74. Turman, B. N. and B. C. Edgar, Global lightning distributions at dawn and dusk, submitted to J. Geophys. Research. See also Edgar, B. C. and B. N. Turman, Optical pulse characteristics of lightning as observed from space, submitted to J. Geophys. Research.

75. Uman, M. A., Y. T. Lin and E. P. Krider, Errors in magnetic direction finding due to non-vertical lightning channels, Radio Sci. 15, 35-39 (1980).

76. Vonnegut, B., C. B. Moore and F. J. Mallahan, Adjustable potential-gradient-measuring apparatus for airplane use, J. Geophys. Res. 66, 2393-2397 (1961).

77. Vonnegut, B. and R. E. Passarelli, Jr., Modified cine sound camera for photographing thunderstorms and recording lightning, J. Appl. Meteor. 17, 1079-1081 (1978).

78. Vonnegut, B., O. H. Vaughan, Jr. and M. Brook, Nighttime/daytime optical survey of lightning and convective phenomena experiment (NOSL), NASA TM-78261 (1980).

79. Warwick, J. W., C. O. Hayenga and J. W. Brosnahan, Interferometric directions of lightning sources at 34 MHz, J. Geophys. Res. 84, 2457-2468 (1979).

80. Watson Watt, R. A. and J. F. Herd, An instantaneous direct-reading radio-goniometer, J. Instn. Elec. Engrs. 64, 611-622 (1926).

81. Weber, M. E. and A. A. Few, A balloon-borne instrument to induce corona currents as a measure of electric fields in thunderclouds, Geophys. Res. Lett. 5, 253-256 (1978).

82. Whipple, F. J. W. and F. J. Scrase, Point discharge in the electric field of the earth, Geophys. Mem. Lond. 68, 1-20 (1936).

83. Wilson, C. T. R., Investigations on Lightning discharges and on the electric field of thunderstorms, Phil. Trans. A221, 73-115 (1920).


DAT
FILM